

**UCSF**

**UC San Francisco Electronic Theses and Dissertations**

**Title**

Characterization of Early Hematopoietic Stem and Progenitor Cell Formation, Maturation, and Function

**Permalink**

<https://escholarship.org/uc/item/2w97h18d>

**Author**

Zape, Joan

**Publication Date**

2017

Peer reviewed|Thesis/dissertation

Characterization of Early Hematopoietic Stem and Progenitor  
Cell Formation, Maturation, and Function

by

Joan Maryl P. Zape

DISSERTATION

Submitted in partial satisfaction of the requirements for the degree of

DOCTOR OF PHILOSOPHY

in

Biomedical Sciences

in the

GRADUATE DIVISION

Copyright 2017  
By  
Joan Maryl P. Zape

## **Dedication and Acknowledgements**

The accomplishment of my PhD training represents my evolution as an individual and as a scientist. My PhD training has given me opportunity to work alongside tireless, dedicated, and creative scientists and researchers, many of whom have become my closest friends. The outcome of my decision to pursue a PhD seven years ago is delightfully unexpected. I am grateful to the people I have met on this journey and for the knowledge and experiences they have shared with me. My life is forever enriched by the lessons I have learned and by the relationships I have cultivated.

First, the work I have accomplished here would not have been possible without the support and encouragement of the scientists around me who have invested their time and energy in guiding my scientific development. I would like to thank my advisor, Ann Zovein, for supporting me throughout the years. I am grateful for her guidance and for allowing me the freedom to pursue my scientific curiosity. Next, I would like to thank members of the Zovein Lab: Carlos Lizama, for assisting me with some very big experiments most of which have contributed directly to the completion of my thesis work, Chris Schmitt for his scientific advice, podcast recommendations and his friendship, Hui Yu, for his tireless work caring for our animal colonies and Sunyoung Wang, for her generous assistance with tedious bone marrow work. I would like to thank my classmate, Megan Robblee, who actually taught me how to do bone marrow extractions and Kelly Cautivo-Reyes who performed tail vein injections and enjoyed escape rooms with me.

I would like to thank my thesis committee chair, Takashi Mikawa, for his guidance and for helping me grow scientifically. I also would like to appreciate my other thesis

committee members, Todd Nystul, for all the insightful and helpful suggestions, and Andy Leavitt for all cheerful discussions of science.

This work would not be possible without the support of my awesome scientist and non-scientist friends. I would like to thank members of the Mikawa Lab, Lisa Hua and Hao Wu, for all the insightful scientific discussions. I am grateful for the science and life advice, for all the free pizza and chocolate chip cookies. I would like to thank Janna Mouw and Laura Damiano for their wise counsel through the challenging times of my training; Zuzka and Marek Vavrusa, Armbien Sabillo and Garrett Smith, for their wonderful friendship.

Finally, I dedicate this thesis work to my Mom and Dad, Daryl and Marianne, who always supported me. I am grateful to all of you for giving me the courage to accomplish the almost-impossible. To my dearest Kate, thank you for always inspiring my curiosity, for the love, and for the awesome adventures throughout all these years.

## **Abstract**

Hemogenic endothelial (HE) cells are a unique subset of vascular endothelial cells endowed with the capacity to generate hematopoietic stem and progenitor cells (HSPCs) through a process called endothelial-to-hematopoietic transition (EHT). This process results in the formation of sizeable HSPC clusters attached to the endothelial wall. While the existence of HE cells is well known, the multi-step process of HSPC cluster formation and maturation following EHT have not been characterized. The dorsal aorta is a well-established hemogenic vascular bed that harbors HSPCs termed intra-aortic hematopoietic clusters (IAHCs). In order to characterize HSPC cluster formation and maturation, I sought to visualize the formation of IAHCs in the dorsal aorta through live-imaging, and to evaluate their cell cycle and proliferation, and their molecular signatures from their initial appearance (E10.5) to the point when cluster cells are capable of adult engraftment (E11.5). I uncovered the dynamic behavior of IAHCs and the appearance of transient filopodial structures, their polyclonal origin of formation, and their distinct temporal molecular signature with differing cell cycle, migration, and cell signaling attributes. In addition, I found that genes of the complement cascade are highly enriched in later IAHCs (E11.5), possibly delineating a new role for this pathway in their maturation and function.

## Table of Contents

<b>Background</b> .....	1
-------------------------	---

### Chapter 1

Intra-aortic hematopoietic clusters form and expand through rapid cell divisions of distinct

hemogenic clones .....	6
------------------------	---

Introduction .....	7
--------------------	---

Materials and Methods .....	8
-----------------------------	---

Results .....	14
---------------	----

Discussion .....	41
------------------	----

### Chapter 2

Intra-aortic hematopoietic clusters contain cells that are positioned at different phases of the cell cycle and have varying engraftment potential during the early and late stages of

the hemogenic window.....	44
---------------------------	----

Introduction .....	45
--------------------	----

Materials and Methods .....	46
-----------------------------	----

Results .....	49
---------------	----

Discussion .....	63
------------------	----

### Chapter 3

Transcriptional profiling of intra-aortic hematopoietic cluster populations across developmental age and cell cycle phase reveals a potential role for complement genes in

the maturation of HSPCs.....	65
------------------------------	----

Introduction .....	66
--------------------	----

Materials and Methods .....	67
-----------------------------	----

Results .....	69
Discussion .....	79
<b>Discussion .....</b>	<b>81</b>
<b>References .....</b>	<b>86</b>

## List of Figures

Figure 1. Experimental set up for the live imaging of aortic slices.....	16
Figure 2. Morphological characteristics of cells in the dorsal aorta.....	17
Figure 3. Live imaging reveals dynamic behavior of pre-formed intra-aortic clusters....	18
Figure 4. PU.1 is a reliable marker of IAHCs during the E10.5 and E11.5 time-points of the hemogenic window.....	21
Figure 5. IAHCs are proliferative and their cell cycle length increases during the later stage of the hemogenic window.....	26
Figure 5 - Supplement. Detection of EdU and BrdU in E10.5 mouse telencephalon.....	28
Figure 6. Low dose clonal labeling of IAHCs reveal clonal heterogeneity and polyclonal origin of IAHCs.....	34
Figure 6 - Supplement. Tamoxifen dose optimization experiments.....	36
Figure 7. Polyclonality of IAHCs is supported using the Cdh5Cre-confetti reporter system.....	39
Figure 8. IAHCs are positioned at different at phases of the cell cycle during E10.5 and E11.5.....	51
Figure 8 - Supplement. Validation of the Fucci System.....	53
Figure 9. Direct transplantation of E10.5 and E11.5 Fucci IAHCs .....	57
Figure 9 - Supplement. Transplantation of donor bone marrow cells as positive control for engraftment.....	59
Figure 10. Transcriptional profiles of E10.5 and E11.5 Fucci IAHCs.....	71

Figure 11. Molecular differences between E11.5 G1 IAHCs and E11.5 S/G2/M IAHCs..... 75

Figure 12. QPCR validation of complement-related genes..... 77

Figure 13. Model of cluster formation and maturation of IAHCs to HSCs..... 85

## List of Tables

Table 1. Estimation of cell number from single clonal divisions at E10.5 and E11.5.....	30
Table 2. Total IAHCs evaluated for clonality at E10.5 and E11.5.....	38
Table 3. Transplantation cell number and engraftment.....	60

## Background

The success of embryonic development is dependent upon the proper formation of the vascular system and the development of hematopoietic stem and progenitor cells (HSPCs) <sup>1</sup>. The hematopoietic system, which develop simultaneously with the initial vasculature, is comprised of hematopoietic stem cells (HSCs), hematopoietic progenitors, and specialized blood and immune cell types <sup>2</sup>. This system of diverse hematopoietic cell types develops from a highly regulated process termed hematopoiesis <sup>2</sup>. This process of producing long-lived blood and immune cell types sustain the embryo during development and throughout adulthood. During ontogeny, the development of a fully functional hematopoietic system occurs in successive waves: the primitive and definitive succession of hematopoiesis.

The primitive wave of hematopoiesis in the mouse initiates in the yolk sac, a bilayer organ composed of extra-embryonic and visceral mesoderm, during embryonic day 7 (E7.0) <sup>3</sup>. This process begins with the production of primitive red blood cells called erythroblasts that are nucleated and that express embryonic globins <sup>4,5</sup> – features that differentiate primitive erythroblasts from their adult definitive counterparts. A typical structure called the “yolk sac blood island” is formed by E8.0. The blood islands comprise of an outer layer of cellular aggregate that assume a spindle shape as the cells differentiate into endothelial cells and an inner layer of cells which become the erythroblasts <sup>3</sup>. Present only for a brief time during development, the hemangioblast was initially thought to be a bi-potential mesodermal progenitor that gives rise to these early blood and endothelial cells <sup>6</sup>. Primitive hematopoiesis also produces primitive macrophage progenitors <sup>7</sup> and

megakaryocyte progenitors<sup>8,9</sup> between E8.5 – E9.0. Together, these early hematopoietic cell types sustain the embryo until a definitive hematopoietic system is established.

The second wave of blood production, termed “definitive hematopoiesis”, is the life-long production of hematopoietic stem and progenitor cells (HSPCs). This process coincides with the onset of circulation beginning at E8.5<sup>10</sup>. During this time, definitive erythroid<sup>11</sup> and myeloid<sup>12</sup> progenitors (EMPs) are also produced in the yolk sac while primitive hematopoietic cells decrease in number<sup>3</sup>. Between E9.0 – E9.5, definitive hematopoiesis occurs in the extra-embryonic placenta<sup>13-15</sup> and between E10 – E10.5, definitive hematopoiesis initiates intra-embryonically in the aorta-gonad mesonephros (AGM) region. Definitive HSPCs emerge from hemogenic endothelium<sup>16-18</sup> and these cells subsequently migrate and colonize the fetal liver by E11 – E12<sup>19</sup>. Finally, by E16.5, HSPCs leave the fetal liver to colonize the bone marrow where they will reside throughout their lifetime<sup>20</sup>.

The cellular origin of HSPCs (including embryonic HSCs) was traced from an endothelial source termed “hemogenic endothelium”<sup>21,22</sup>. The concept first began with observations that initially supported the hypothesis of the hemangioblast. In 1917, anatomist Florence Sabin, noted the close association between the red blood cells and the endothelium of the blood vessels in the chick<sup>23</sup>. After a century of research, it is now established that the hemangioblast gives rise to HSPCs through a hemogenic endothelial cell intermediate<sup>24</sup>.

HE cells are especially endowed with the capacity to generate the first definitive HSPCs of the body, and this ability exists transiently during a narrow window (E9.5 to E11.5) in development<sup>21 22,25 26 18</sup>. Hemogenic vascular beds include the AGM<sup>17,21,27,28</sup>, placenta<sup>14,29</sup>, and umbilical and vitelline arteries<sup>18,30,31</sup>. Recent studies have also detected hemogenic endothelium in the developing endocardium<sup>32,33</sup> and cranial vessels of the head<sup>34,35</sup>.

HE cells give rise to hematopoietic cells through a process called endothelial-to-hematopoietic transition (EHT)<sup>36</sup>. This transformation of endothelial cells to blood cells is characterized by their loss of cell-cell adhesion and the subsequent rounding-up of their morphology<sup>36</sup>. Recent studies have shown that, Runx1, a critical regulator for hematopoiesis, is critical to hemogenic endothelium<sup>37</sup> and EHT<sup>36</sup>. Furthermore, Gpr56, a G-protein coupled receptor, was also demonstrated to be important for EHT<sup>38</sup>. Following the process of EHT, a cluster of hematopoietic cells is observed to bud off of the endothelial wall. These hematopoietic clusters are the unique identifying feature of hemogenic vasculature.

As the most extensively studied hemogenic vascular bed, the AGM contains hematopoietic clusters termed intra-aortic hematopoietic clusters (IAHCs). While the AGM region has long been shown to engraft irradiated adult host<sup>16,17,39</sup>, transplantation of isolated IAHCs has only been recently carried out with sorted SSEA-1<sup>-</sup>/CD31<sup>+</sup>/CD117<sup>+</sup> cells (IAHC populations) from E11.5 AGMs that were shown to engraft irradiated adults<sup>40</sup>. Thus, the IAHC population contains bona fide definitive HSCs in addition to progenitor

cells. Transplantation of the same cell population from E10.5 AGMs (one day earlier), however, shows undetectable repopulation activity in adult irradiated mice <sup>16,40,41</sup>, but does demonstrate engraftment of neonates <sup>42,43</sup>. The neonatal engraftment at E10.5 suggests that the IAHCs also contain hematopoietic stem and progenitor cells, but that the HSC population is immature or a pre-HSC population <sup>42,43</sup>. These studies demonstrate that IAHC populations only possess adult engraftment potential later in the HE time window, and suggest a maturation process from E10 to E11 that allows for adult engraftment. Since the production of HSPCs during development occurs during a narrow period, concerted spatial and temporal control may govern the process of pre-HSC maturation. Therefore, the characterization of the subsequent steps after EHT that lead to hematopoietic cluster formation and its impact on HSPC maturation are of importance to the field, and will enable our understanding of embryonic HSC development and maturation from HE.

The goal of this dissertation is to investigate the formation of hematopoietic clusters in the AGM and to further define the relationship of this group of hematopoietic cells with the emergence of the first HSCs in the embryo. In Chapter 1, I used live-imaging to observe the morphology and behavior of IAHCs in their near-native environment. I also show the proliferation and polyclonality of IAHCs as contributors to IAHC formation and expansion during the pre-HSC (E10.5) and HSC (E11.5) periods of the hemogenic window. In Chapter 2, I found that IAHCs are positioned at different phases of the cell cycle during these two time-points of the hemogenic window and that IAHCs from the later hemogenic time-point (E11.5) contain transplantable HSCs that may be enriched in

the G1 phase of the cell cycle. Finally, in Chapter 3, I examined the transcriptional landscape of IAHCs across their developmental age and cell cycle phase, and uncovered the potential role of complement in the development and maturation of embryonic HSCs from IAHCs. These findings contribute to the field's understanding of embryonic HSC development and reconcile the emergence of HSCs in the AGM with a maturation process of HSPCs contained in the IAHCs.

## **CHAPTER 1**

**Intra-aortic hematopoietic clusters form and expand through rapid cell divisions  
of distinct hemogenic clones**

## Introduction

Hematopoietic clusters uniquely identify the presence of hemogenic endothelium<sup>21,22</sup>. IAHCs appear at E10.5 and embryonic HSCs are detectable by E11.5. Transplantation experiments of sorted E10.5 IAHC (SSEA-1<sup>-</sup>CD31<sup>+</sup>CD117<sup>+</sup>) population showed only neonatal engraftment and no detectable engraftment of adult recipients<sup>40</sup>. Transplantation of E11.5 IAHC populations, however, demonstrated reconstitution of adult irradiated animals<sup>40</sup> suggesting the presence of a bona fide HSC population. Moreover, mice deficient for transcription factor, Runx1, are devoid of IAHCs during development and consequently, HSCs<sup>27,44,45</sup>. These observations suggested a maturation process from IAHCs to HSCs that begin from E10.5 to E11.5 of the hemogenic window. The subsequent processes of IAHC cluster formation following EHT and details of their maturation towards an HSC identity remain unclear. Recent findings added that the maturation step towards an HSC fate involved low cell proliferation<sup>42</sup>. The data that supported this observation was based on the examination of the mitotic index of IAHCs using phospho-histone3 (pH3) as a marker of proliferation. However, one drawback of using the mitotic index as a measure of proliferation is that the M-phase is generally the shortest phase of the cell cycle and cells traverse this phase at a faster rate than any other phase of the cell cycle. Therefore, while mitotic cells appear to be rare, cells that are actively proliferating may not be. In order to characterize the formation and maturation of IAHCs to HSPCs, I first examined the formation of IAHCs following EHT in the AGM. In this chapter, I developed a live-imaging technique to visualize the formation of IAHCs.

Furthermore, I investigated the cell proliferation of IAHCs and the extent their clonality contributed to the expansion of their cell size (number).

## **Materials and Methods**

### ***Mice***

Mice were housed under a barrier facility following IACUC procedures and animal protocols were conducted under the University of California San Francisco Laboratory Guidelines. C57/Bl6 (Wildtype) females were crossed with Wildtype males to obtain E10.5 embryos. Similarly, *Gt(ROSA)26Sortm4(ACTB-tdTomato,-EGFP)Luo/J*<sup>46</sup> (R26r-mTmG), *Gt(ROSA)26Sortm1(CAG Brainbow2.1)Cle/J* (R26r-confetti)<sup>47</sup>, were crossed with *Cdh5(PAC)-CreERT2 (Tg(Cdh5-cre/ERT2)1Rha) (iCdh5-Cre)*<sup>48</sup> and *Tg(Cdh5-Cre)1Spe (VE-cadherinCre)*<sup>37</sup> and *Gt(ROSA)26Sortm9(CAG-tdTomato)Hze* (R26r-tdTomato)<sup>49</sup> to obtain E10.5 labeled embryos. Pregnancies were timed in accordance with the vaginal plug (gestation day 0.5 on the day of the plug). Genomic DNA from adult tail tips or conceptus yolk sacs was genotyped using MyTaq Extract PCR Kit (Bioline, BIO21127) according to manufacturer's instructions.

### ***Genotyping***

#### ***Cre PCR Program***

95°C x 3 min, 95°C x 15s, 55°C x 15s, 72°C x 30s repeat for 34 cycles, 72°C x 5 min, and hold at 4°C infinitely.

#### ***mTmG PCR Program***

95°C x 3 min, 95°C x 15s, 59°C x 15s, 72°C x 30s repeat for 34 cycles, 72°C x 5 min, and hold at 4°C infinitely.

#### ***Brainbow PCR Program***

94°C x 3 min, 94°C x 30s, 58°C x 30s, 72°C x 30s repeat for 35 cycles, 72°C x 2 min, and hold at 4°C infinitely.

## **Primers**

Primer stock concentrations were prepared at 100  $\mu$ M. A 10x dilution is performed to prepare working concentrations of 10  $\mu$ M. Primers were stored in -20°C.

Name	Forward Primer	Reverse Primer	Additional Primer
Cre	5'-CCA-AAA-TTT-GCC-TGC-ATT-ACC-GGT-CGA-TGC-3'	5'-ATC-CAG-GTT-ACG-GAT-ATA-GT-3'	
mTmG	5'-CTC-TGC-TGC-CTC-CTG- GCT-TCT-3'	5'-CGA-GGC-GGA-TCA-CAA-GCA-ATA-3'	5'-TCA-ATG-GGC-GGG-GGT-CGT-T-3'
Brainbow	5'-GAA-TTA-ATT-CCG-GTA-TAA-CTT-CG-3'	5'-AAA-GTC-GCT-CTG-AGT-TGT-TAT-3'	5'-CCA-GAT-GAC-TAC-CTA-TCC-TC-3'

## **Vibratome Sectioning**

100 ml of 4% low melting agarose (LMA) was prepared by mixing 4 g of LMA with 100 ml of 1x PBS and 1% LMA was prepared by mixing 1 g of LMA with 1 ml of 1x PBS. The solution was heated in the microwave for 3 minutes until the LMA was dissolved. The solution was then cooled and poured into metal molds and the embryos embedded in the center of the mold. This was followed by cooling the gel on ice for 5 minutes. When solidified, edges of the mold were trimmed into a small square using a clean blade. The gel was mounted on the vibratome stage, attached with a Krazy glue, and left to dry at room temperature for one minute. The vibratome chamber was then filled with ice cold 1x PBS and slices were sectioned in 300  $\mu$ m using a sapphire blade. Loose vibratome sections were collected in a 10 mm glass bottom dish with 1x PBS and were remounted in 1% LMA. Samples were covered with 1 ml complete MCDB-121 media for 2 hours.

## **Live Imaging**

Prior to imaging, the media was replaced with Hank's Balanced Salt Solution supplemented with 2% serum, 1% P/S and 20  $\mu$ M of HEPES. Live-imaging was taken using a 40x objective on an inverted Nikon Microscope or 20x objective using an inverted Zeiss Microscope equipped with a controlled tissue culture environment (See Figure 1).

### ***Low density clonal labeling***

Pregnant female mice were with intraperitoneally injected with single 0.05 mg, 0.1 mg or 0.15 mg doses of tamoxifen at E8.5 prior to cluster formation to determine the optimal dose for clonal labeling. Embryos were evaluated at E10.5 and/or E11.5.

### ***Tamoxifen Preparation***

Tamoxifen was purchased from MP Biologicals LLP. A 10mg/ml stock was prepared by dissolving 10 mg of tamoxifen in 100 $\mu$ l of 100% ethanol mixed with 900 $\mu$ l sunflower oil (1:9). For low dose clonal labeling experiments, a stock solution of 2.5mg/ml of tamoxifen was prepared in similar fashion but dissolving 2.5 mg of tamoxifen.

### ***Cell Cycle Length Determination***

Cell cycle length was determined by sequential administration of EdU and BrdU. First, 1.5 mg of EdU (10 mg/ml) was administered intraperitoneally. After 1.5 hours, 2 mg of BrdU (10mg/ml) was injected which was allowed to circulate for 30 minutes. Embryos were then collected, cryopreserved, and analyzed. BrdU was detected by treating tissue sections with pre-warmed 2N HCl for 30 minutes at 37°C and was subsequently neutralized in 0.1M of boric acid for 15 minutes at room temperature. Samples were then incubated with 1:100 anti-BrdU (MOBU-1, Life Technologies #B35128). Samples were washed 3x with 1x PBS + 0.05% Tween (PBST) and a secondary antibody was applied at 1:200 (Invitrogen, #A21203). EdU was detected using a Click-iT EdU Detection System (Life

Technologies, #C10337) following manufacturer's instructions.

### ***Flow Cytometry***

Whole embryos or AGMs were first mechanically dissociated using a P200 by pipetting up and down 15x, followed by dissociation using P1000 15x. Dissociated samples were then incubated in 20 µg/ml of DNase I (1 mg/ml stock) and 20 µg/ml of Collagenase I (1 mg/ml stock) for 15 minutes at 37°C. Samples were then spun down at 2000 RPM and resuspended in 400µl of Hank's Balanced Salt Solution with 2% FCS and 2% HEPES (FACS buffer). Samples were stained with FACS antibodies for 30 min at 4°C with agitation and were washed in 1x FACS buffer. Single cell suspensions were sorted in a BD FACS Aria III. Flow cytometric analyses were performed on a FACS Verse or FACS Aria III with FACSDiva 8.0 software (BD Biosciences) and the data was analyzed using FlowJo v10.0.7 (Tree Star).

### ***FACS Antibodies***

Antibodies were purchased from BD Biosciences: CD117-APC (#553356), CD31-PerCPy5.5 (#562861), V450-SSEA-1 (#561561), APC-CD45.2 (#558702), FITC-CD45.1 (#553775), PeCy7-CD11b (#552850), FITC-CD3 (#55274), PE-Ter119 (#553673). Isotype controls used were: IgG2b-APC (#55391), IgM-V450 (#560861), IgG1-PerCPy5.5 (#562861), IgG2b-PeCy7 (#552849), IgG2b-FITC (#553988), IgG2b-PE (#553989). Antibodies were purchased from Biolegend: PE-CD45R/B220 (#103208) and IgG2a-PE (#400507).

### ***Immunofluorescence and confocal microscopy***

E10.5 - E11.5 embryos were fixed in 4% paraformaldehyde (PFA) solution at room temperature for 20 minutes or in 2% PFA overnight. Samples were frozen in Tissue-Tek

OCT Compound (Sakura Finetek, 4583). 20-30  $\mu\text{m}$  cryosections were obtained (Thermo Scientific Micron, HM550). Slides were incubated in blocking buffer (PBS, 0.5% Triton-X100) with 5% serum for 1 hour. Primary antibodies were incubated at 4°C overnight or room temperature for 2 hours in blocking buffer. Slides were washed (PBS 0.05% Tween), incubated with the secondary antibodies for 1 hour, stained with 2 $\mu\text{g}/\mu\text{l}$  DAPI and mounted in Vectamount (Vector Laboratories, H-5000). Images were captured on a Leica SPE Confocal Microscope.

### ***Immunofluorescence Antibodies***

For immunofluorescence experiments 1:100 of Rabbit Runx1 (ab35962), Goat Sox17 (R&D Systems #AF1924) Rat CD117 Clone (2B8) BD Pharmingen (#553352) Rat CD31 Clone (Mec13.3) BD Pharmingen (#553370) Rabbit PU.1 Clone (9G7) Cell Signaling (#2258) were utilized. Secondary antibodies according to host species were used at 1:200 dilutions (Invitrogen: donkey anti-goat 488 #A11055, donkey anti-rat 594 #A21209, donkey anti-rabbit 647 #A31573).

### ***Image Analysis and Cluster Quantification***

Immunofluorescence of R26R-mTmG, R26R-confetti, and wild type sections were taken on a Leica SPE/SP5 confocal microscope with a 40x oil objective. Immunofluorescence of FUCCI sections were taken on Leica SP5 confocal microscope with a 40x oil objective. All reconstructions were generated from z-stacks using the Imaris software [Imaris 8.6] (Bitplane; Belfast, UK). Images are a maximum projection of 30-40  $\mu\text{m}$  cryoslices. A Gaussian filter is applied to all images. IAHG cluster cell number counts were done based on nuclear PU.1, with endothelial labelling of SOX17 with the addition of CD31.

## Results

### *Live imaging of mouse dorsal aorta reveals dynamic behavior of intra-aortic clusters*

To visualize the formation of IAHCs in the dorsal aorta in real-time, I adapted and optimized a live-imaging protocol from Boisset et al. (Figure 1)<sup>50</sup>. I performed live imaging experiments in 300  $\mu\text{m}$  dorsal aortic sections of wild type mice during the active hemogenic window at E10.5 (Figure 2A). The data showed the initial emergence of a rounded cell from the ventral floor of the aorta (Figure 2A). This observation validated my technical set up and demonstrated that IAHCs arise from hemogenic endothelial cells in the ventral floor of the aorta. To obtain better contrast, live imaging experiments were performed using labeled mouse lines. First, I used a constitutive VE-cadherinCre-Tdtomato to label all endothelial cells (Figure 2B). In this live-imaging experiment, the data showed a single rounded cell at the beginning of the time-lapse. In the subsequent frame (Frame 11), this labelled rounded cell appeared to extended a thick filopodia-like protrusion (Figure 2B). Subsequently, another filopodial protrusion appeared in the foreground though the cell body appeared invisible. This structure appeared narrower compared to the first protrusion in frame 11 of the time-lapse. Interestingly, frames 35-44 (Figure 2B) showed that several cells in the aortic floor contained these thin, filopodial protrusions resembling that of a cytoplasmic bridge. Overall, this data demonstrates, for the first time, the appearance of transient filopodial structures (Figure 2C) from labeled cells in the dorsal aorta. Separately, using an inducible Cdh5Cre-mTmG reporter, the data showed the behavior of two adjacent clusters beginning from time 0 up to 20 hours

(Figure 3A). The videos depicted that IAHCs from the left cluster had given rise to a small cluster of 2-3 cells (Figure 3A). This small group of cells interacted with the cells in the IAHC on the right. Interestingly, in the frame timed 13:00:00, a green cell extended a filopodia-like structure towards the newly formed group of 2-3 cells. This extension fragmented as it enveloped these newly formed the cells (Figure 3A). Overall, these data suggest that IAHCs display dynamic morphology and behavior during development.

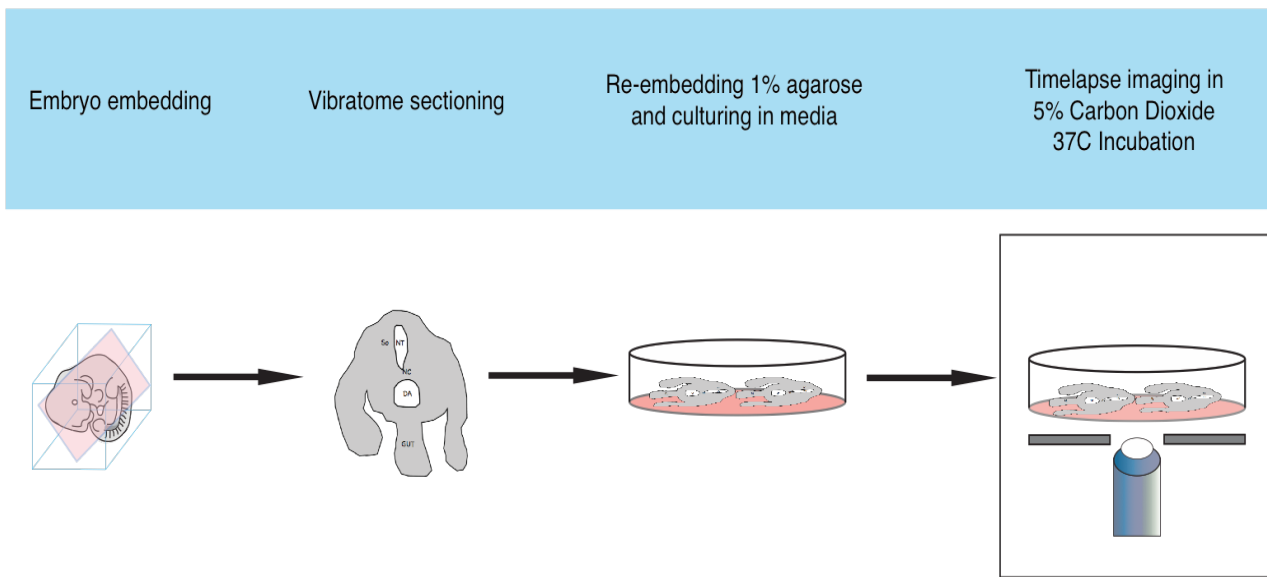


**Figure 1. Experimental setup for the live imaging of aortic slices.**

Embryos were embedded in 4% low melting agarose in a metal mold. Sections were created by mounting the mold in the stage and were transversally cut in 300  $\mu\text{m}$  thickness using a sapphire vibratome blade. Subsequently, samples were collected in a 10 mm glass bottom dish and were re-embedded in 1% low melting agarose. Complete MCDB-121 media was then used to culture the samples for 2 hours in tissue culture conditions (37°, 5%  $\text{CO}_2$ ) and was then replaced by a clear Hank's Balanced Salt Solution supplemented with 2% FBS. An inverted spinning disk microscope was used for live-imaging and samples were imaged in tissue culture conditions.

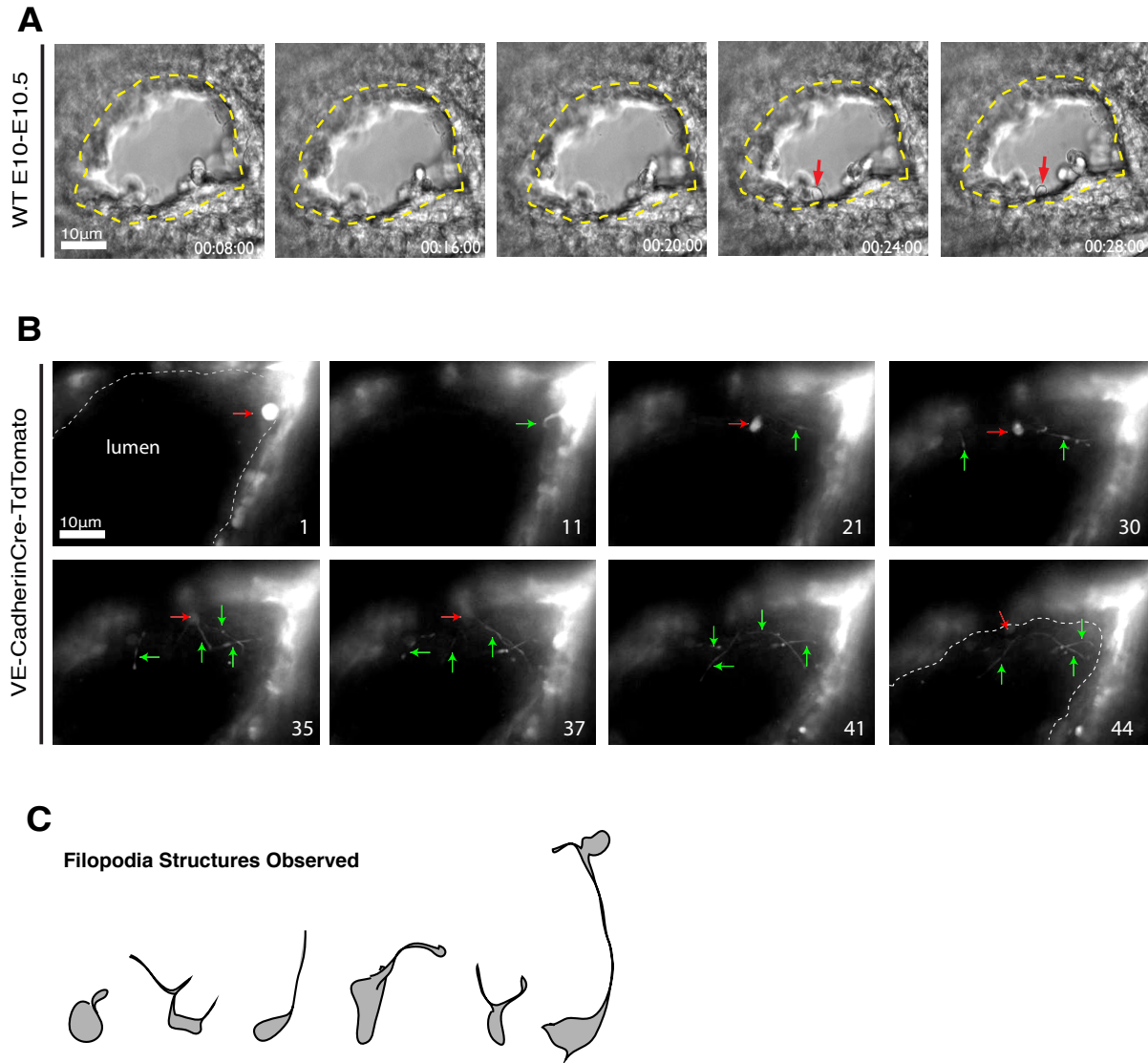


**Figure 2. Morphological characteristics of cells in the dorsal aorta.**

(A) Live imaging of wild-type E10.5 dorsal aorta. Video snapshots from 8 to 28 minutes show the emergence of a rounded cell from the ventral floor. Yellow broken line denotes endothelium. Red arrow denotes emerging cell. (B) Live-imaging of the dorsal aorta from VE-CadherinCre-tdTomato animal shows a rounded cell and the appearance of different filopodia-like structures. Frame 1 shows a rounded cell (red arrow). Frame 11 shows a filopodia-like extension (green arrow). Frame 21-30 shows a cell body (red) with delicate cellular extensions. Frame 35-44 shows the appearance of several, long filpodia-like extensions from labeled cells in the dorsal aorta. Note that each frame is taken at 15 minute intervals over 10 hours. (C) Graphic depiction of different filopodia-like structures observed. Scale bars, 10  $\mu$ m.

**A**

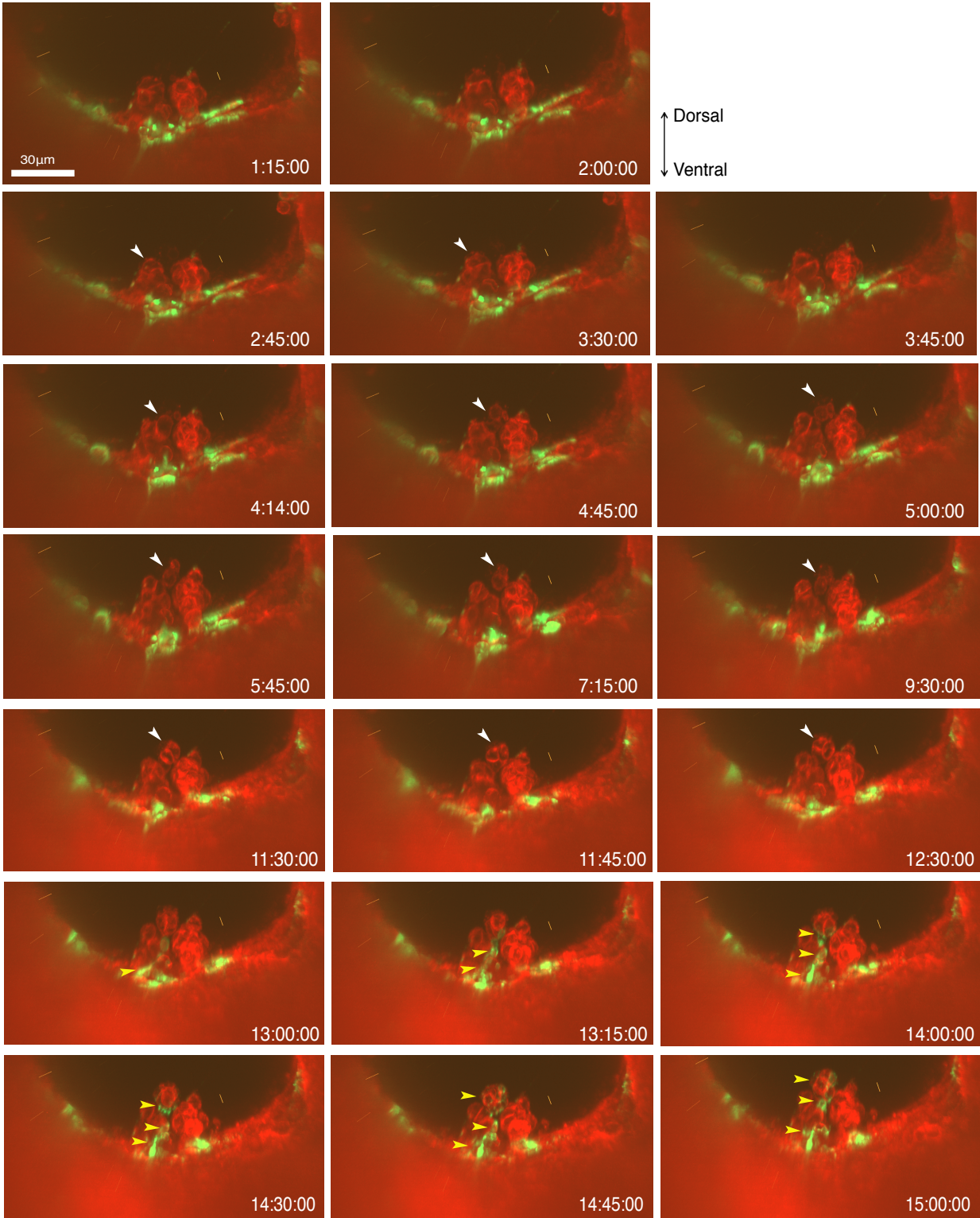


**Figure 3. Live imaging reveals dynamic behavior of pre-formed intra-aortic clusters in the dorsal aorta.**

(A) Live-imaging of Cdh5Cre-mTmG dorsal aorta. Visualization of pre-formed intra-aortic clusters using the inducible Cdh5Cre-mTmG reveals cell division in the IAHC and filopodia-like extension from a labeled cell. Time frames 1:15:00 to 3:45:00 follows a dividing cell which will form a new group of 2-3 cells (white arrows). Time frames 4:15:00 to 12:30:00 follows the interaction of the newly divided cells (white arrows) with the adjacent IAHCs on the right. Time frames 13:00:00 to 15:00:00 depicts the appearance of a labeled cell (yellow arrow) extending a filopodia-like structure to envelop the newly divided cells. Each frame was taken every 15 minutes over 20 hours. Scale bars, 30  $\mu$ m.

### ***PU.1 is a reliable marker of IAHCs***

While live imaging of IAHCs provided insight into their different cellular morphologies and behavior, technical limitations such as inconsistent observations among different sections and photo-bleaching have made it challenging to accurately interpret these results. Because of these hurdles, I decided to use a combination of various experimental methods to study IAHC formation. First, a reliable nuclear marker was needed to label IAHCs exclusively from hemogenic endothelial cells. From initial observations of wild type E10.5 embryos using immunofluorescence, I visualized the expression RUNX1 and SOX17, a critical transcription factor for hemogenic endothelium and an arterial marker, respectively. Figure 4A shows the localization of RUNX1 to cells in the IAHCs (Figure 4A, white arrow) and in some endothelial cells (Figure 4A, yellow arrow heads). SOX17 localized to only endothelial cells (Figure 4A, white arrow heads) and was absent in IAHCs (Figure 4A, white arrow). The presence of RUNX1 in IAHCs suggested that perhaps other downstream targets of RUNX1 may mark IAHCs exclusively. Wilkinson et al., through single cell analysis, identified PU.1 as being necessary for hematopoietic specification<sup>51</sup>. PU.1-lacZ animals generated in the study showed localized expression in IAHCs of the dorsal aorta. Moreover, PU.1 is a well-known target of RUNX1<sup>52</sup>. To investigate if PU.1 marked IAHCs exclusively, I performed immunofluorescence to visualize PU.1 in E10.5 the dorsal aorta. Figure 4B showed that PU.1 localized to IAHCs exclusively and in some single SOX17<sup>-</sup> cells on the endothelial floor. Quantification of clusters with PU.1 revealed that >95% of IAHCs are PU.1<sup>+</sup> (Figure 4C, D). Moreover, examination of PU.1 in E11.5

IAHCs also revealed similar percentages of PU.1<sup>+</sup> IAHCs (Figure 4C, D). Collectively, these data suggest that PU.1 is a reliable marker of IAHCs.

To characterize the formation of IAHCs, I first established a definition of an IAHC as group of 3 or more cells. I utilized PU.1 as a marker for IAHCs and examined their distribution according to their cell number (cluster size) during the different periods of the hemogenic window (E10.5 and E11.5). Quantification of IAHCs at E10.5 revealed a wide distribution of IAHC size that ranged from IAHCs with 3 cells to 47 cells (Figure 4E). Interestingly, at E11.5 the distribution range of IAHCs decreased from 3 cells to 11 cells (Figure 4F). The data also show that most frequently, IAHCs are composed of 3 cells and that larger IAHCs (>10 cells) are a rarity. Collectively, these data suggest that a majority of IAHCs is produced at E10.5, the time point thought to be the peak of IAHC formation<sup>40</sup> and that IAHC formation decreases with time.

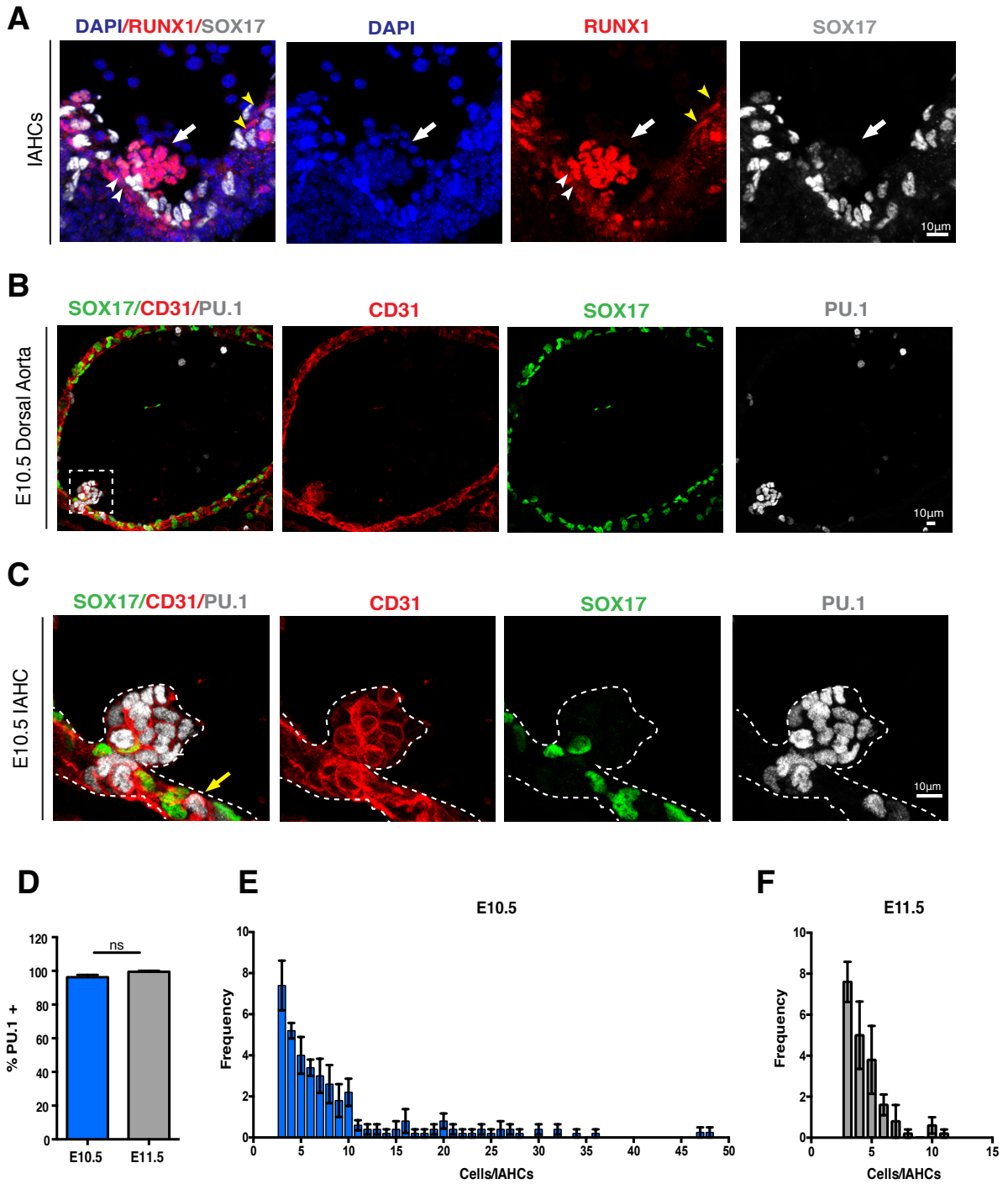


**Figure 4. PU.1 is a reliable marker of IAHCs during the E10.5 and E11.5 time-points of the hemogenic window**

(A) Immunofluorescence of the dorsal aorta. SOX17 (gray) and RUNX1 (red) marks endothelial cells and IAHCs. RUNX1 marks both endothelial cells and IAHCs. While

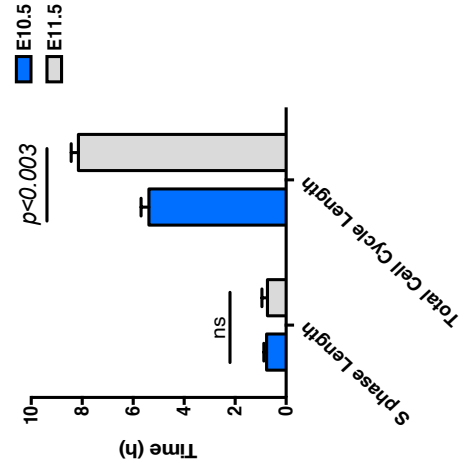
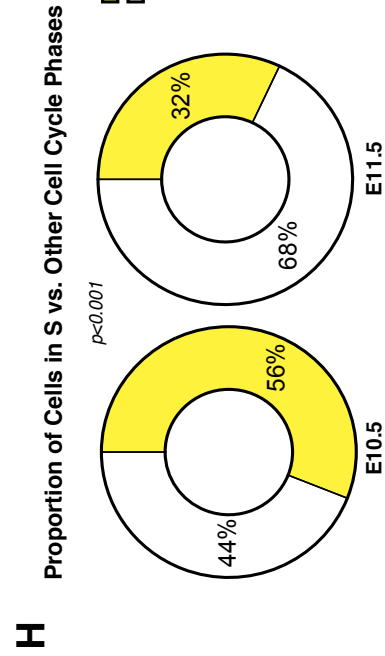
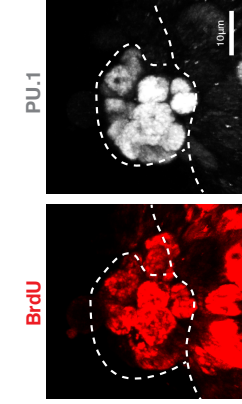
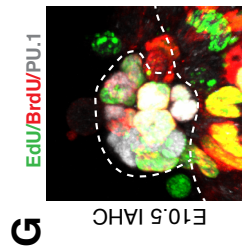
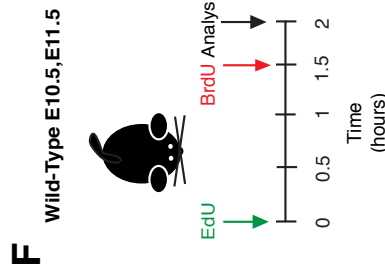
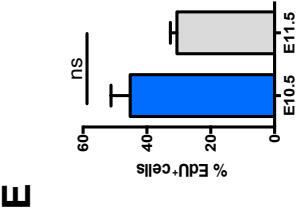
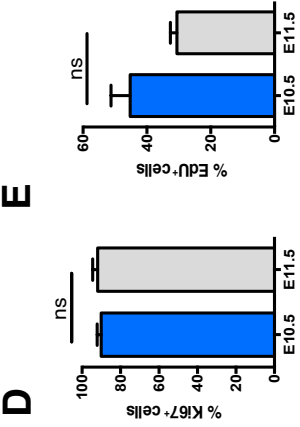
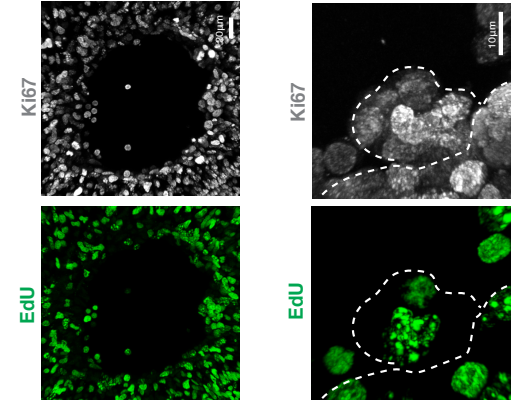
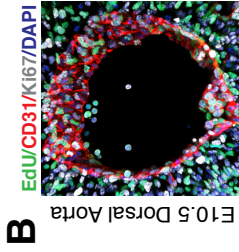
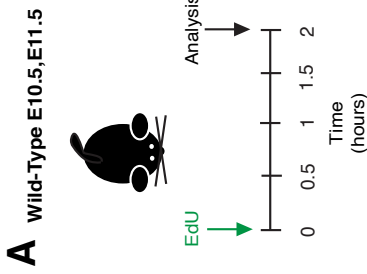
SOX17 is an exclusive arterial endothelial cell marker. Immunofluorescence of the dorsal aorta. (B) Immunofluorescence of the dorsal aorta. SOX17 (green) and CD31 (red) marks endothelial cells. PU.1 (grey) strongly marks the hematopoietic cluster (white arrow) and weakly marks some SOX17<sup>-</sup> single cells in the endothelial layer (yellow arrow). Scale bars, 10  $\mu$ m. (C) Close up view of IAHCs. PU.1 marks cells in the hematopoietic cluster and some SOX17<sup>-</sup> single cells in the endothelial layer (yellow arrow). Scale bars, 10  $\mu$ m. (D) Quantification of IAHCs containing cells marked with PU.1 shows >90% of IAHCs examined were PU.1<sup>+</sup> at E10.5 (n=3, 71 IAHCs) and E11.5 (n=3, 51 IAHCs). (E) Distribution of cluster size at E10.5 shows that IAHC size have wide distribution range from 3-47 cells. n=5, 190 IAHCs (F) Distribution of cluster size at E11.5 shows a decrease in the range of IAHC size to 3-11 cells. n=5, 99 IAHCs.

### ***Cell Cycle Kinetics of IAHCs Reveal Rapid Proliferation and Expansion of IAHCs***

Since I observed that IAHCs could be  $\geq 20$  cells, I next determined the extent cell proliferation contributed to the formation of IAHCs. First, to determine if IAHCs are proliferative, I injected the nucleoside analog, 5-ethynyl-2'-deoxyuridine (EdU), to pregnant females at E10.5 and separately at E11.5, and evaluated embryos 2 hours after (Figure 5A). Immunofluorescence for EdU distinguishes cells in the S-phase from cells in other phases of the cell cycle<sup>53,54</sup>, and Ki67 labels cells in all active phases of the cell cycle (except  $G_0$ )<sup>55</sup>. The analysis revealed highly proliferative cells in the IAHCs (Figure 5B, C). Moreover, quantification of IAHCs that express these markers showed that  $\sim 90\%$  of cells in IAHCs were Ki67<sup>+</sup>, and  $\sim 42\%$  of these cycling IAHC cells were EdU<sup>+</sup> (Figure 5D, E). These percentages were similar upon examination of E11.5 IAHCs (Figure 5D, E). Together, these data show that these two points in the hemogenic window contain IAHC cells that are highly proliferative.

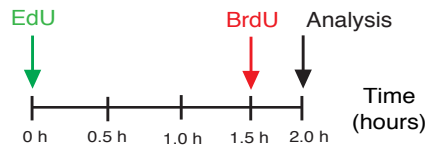
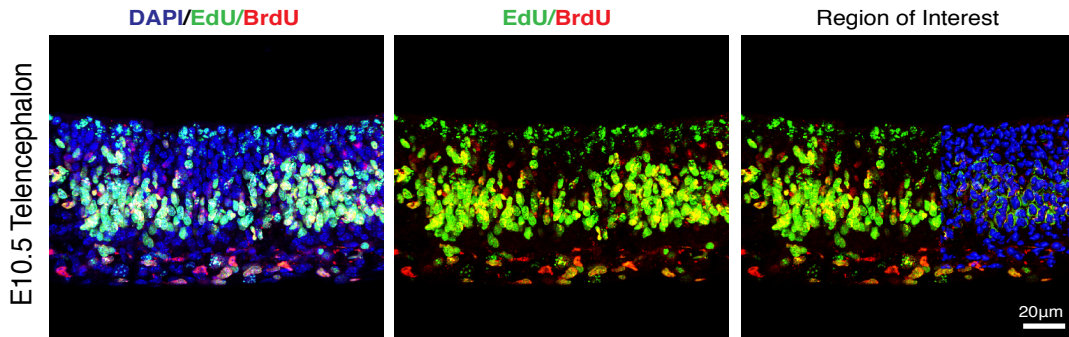
Since IAHCs contain highly proliferative cells, I then estimated their average generation time (total cell cycle length). I labelled IAHCs with a sequential pulse of nucleoside analogs, 5-ethynyl-2'-deoxyuridine (EdU) followed by 5-bromo-2'-deoxyuridine (BrdU)<sup>56,57</sup> (Figure 5F). The sequential administration of these compounds allows for the determination of the cell cycle kinetics of proliferating IAHCs by separating cells into the earliest (EdU<sup>-</sup>BrdU<sup>+</sup>), mid (EdU<sup>+</sup>BrdU<sup>+</sup>) and late (EdU<sup>+</sup>BrdU<sup>-</sup>) S phase. To validate the system, I evaluated EdU and BrdU in the neural tube at E10.5 (Figure S5) and noted comparable numbers to a previous report<sup>57</sup> (Figure S5). To adapt the system

for IAHC evaluation, I utilized PU.1 as a nuclear marker of IAHCs (Figure 4)<sup>51</sup> which I had previously determined to contain about ~90% Ki67<sup>+</sup> cells, as an estimate of the total number of proliferating cells (Figure 5A-E). Analysis of the dual pulse labeling revealed that majority of the cells in IAHCs at E10.5 were positioned in the S-phase, while a majority of IAHC cells at E11.5 were positioned elsewhere in the cell cycle (E10.5 vs. E11.5,  $p < 0.001$ ) (Figure 5G, H). Furthermore, I estimated the total length of the cell cycle ( $T_c$ ) of IAHCs at E10.5 to be 5.38 hours and the S-phase length ( $T_s$ ) at 0.78 hours (Figure 5I). To further gain insight into the cell cycle kinetics of IAHCs, I extended this analysis to E11.5, and found that the  $T_c$  lengthened to 8.16 hours ( $T_c$  E10.5 vs E11.5,  $p < 0.003$ ) while the  $T_s$  remained the same ( $T_s$  E10.5 0.78 h vs. E11.5 0.74 h) (Figure 5I). Overall, these data suggest that IAHCs are capable of dividing 4.5 times within a 24-hour period of time leading to the peak of the hemogenic window (E10.5), such that a single clone cycling at the peak rate could engender up to 22.6 cells or 23 cells (Table 1). Furthermore, these observations also suggest that cell division alone from a single hemogenic clone could not account for IAHCs with greater than 23 cells.



**Figure 5. IAHCs are proliferative and their cell cycle length increases during the later stage of the hemogenic window.**

(A) EdU labeling experimental schema. Pregnant wildtype animals at E10.5 and E11.5 were injected intraperitoneally (IP) with 1.5 mg of EdU two hours before evaluation of embryos. (B) Immunofluorescence of proliferation markers, EdU an S-phase marker (green) and Ki67, a general proliferation marker (expect G<sub>0</sub>) (grey) in the dorsal aorta at E10.5. CD31 (red) delineates the endothelium. The white dotted box outlines an IAHc. Scale bar, 20  $\mu$ m. (C) Higher magnification of an E10.5 IAHc containing labeled EdU<sup>+</sup> and Ki67<sup>+</sup> cells. CD31 marks the endothelium and IAHcs. Scale bar, 10  $\mu$ m. (D) Quantification of Ki67<sup>+</sup> cells in IAHcs expressed as percentage of total cells. (E10.5 mean = 90.1% vs E11.5 mean = 83.46% p=0.50) (E) Quantification of EdU<sup>+</sup> cells in IAHcs expressed as the percentage of the total number of Ki67<sup>+</sup> cells. (E10.5 mean = 45.2% vs E11.5 mean = 27.9% p=0.081. A total of n = 47 IAHcs were analyzed at E10.5 and a total of n = 44 IAHcs were analyzed at E11.5. (F) EdU and BrdU sequential labeling experimental schema. Pregnant wildtype animals at E10.5 and E11.5 were sequentially pulsed with EdU followed by BrdU. 1.5 hours apart. This technique allows for identification of cells that are in the S-phase (S) (EdU<sup>+</sup>BrdU<sup>+</sup>) and cells leaving the S-phase (L) (EdU<sup>+</sup>BrdU<sup>-</sup>). All proliferating IAHc cells are marked by PU.1. The total length of S phase is estimated by first calculating the number of cells leaving the S-phase (L) over the total number of cells in the S-phase (S). The initial time (Ti) between EdU and BrdU (1.5hrs) is then divided by this fraction. The total length of the cell cycle (Tc) is estimated by first determining the number of cells in the S-phase over the total number of proliferating cells (P). The total S-phase length (Ts) is then divided by this fraction. (G) Immunofluorescence of an IAHc containing EdU<sup>+</sup> (green) and BrdU<sup>+</sup> (red) cells. PU.1 (grey) was used to distinguish IAHcs. This representative image depicts an IAHc that contains cells at different phases of the cell cycle given their varying incorporation of EdU (green), BrdU (red) or both (yellow). A total of 81 IAHcs were evaluated at E10.5 and a total of 87 IAHcs were evaluated at E11.5. Scale bar, 10  $\mu$ m. (H) Comparison of the proportion of cells in the S phase (EdU<sup>+</sup>BrdU<sup>+</sup>, yellow) versus other cell cycle phases during E10.5 and E11.5 (Fisher's exact test, p<0.001). At E10.5 most IAHcs contain cells that are in S phase (56% S-phase vs. 44% other phases) while at E11.5, most IAHcs contain cells in the other phases of cell cycle (32% S-phase vs. 68% other phases). (I) Comparison of the S-phase length between E10.5 and E11.5 shows no difference (0.78h vs 0.74h, t-test with Welch's correction p<0.9). Comparison of the total cell cycle length between E10.5 and E11.5 demonstrates lengthening of the cell cycle (5.38h vs 8.16h, t-test with Welch's correction p<0.003). All data shown as mean +/- SEM. All experiments were conducted with n=2-3 litters.

**A****Wild-Type E10.5****B****C**

Parameters for estimating the cell cycle length	
DAPI (P)	183 cells
EdU+BrdU+ (S)	49 cells
EdU+ BrdU- (L)	38 cells
Ti	1.5 hours
<b>Ts</b>	<b>2 hours</b>
<b>Tc</b>	<b>7.2 hours</b>

**Figure 5 – Supplement. Detection of EdU and BrdU on E10.5 mouse telencephalon.**

(A) EdU and BrdU sequential labeling experimental schema. Pregnant wildtype animals at E10.5 and E11.5 were sequentially pulsed with EdU followed by BrdU 1.5 hours apart. (B) Immunofluorescence of EdU (green) and BrdU (red), with DAPI (blue) in the mouse telencephalon at E10.5. Scale bar, 20  $\mu$ m. (C) Quantification of the total cell cycle length

and S phase length. Cells in the telencephalon are labeled with DAPI (blue). Cells in the S phase are EdU<sup>+</sup>BrdU<sup>+</sup>, and cells leaving the S phase are EdU<sup>+</sup>BrdU<sup>-</sup>. Total S phase length in the telencephalon is estimated to be around 2 hours (vs. 4 hours)<sup>57</sup> and the total cell cycle length is estimated to be around 7.2 hours (vs. 7 hours)<sup>57</sup>.

**Table 1. Estimation of Cell Number from Single Clonal Divisions at E10.5 and E11.5**

<b>Age</b>	<b>Tc (h)</b>	<b>Window</b>	<b>Cell Divisions</b>	<b># of cells from single clone</b>
E10.5	5.38	24	4.46	22.02
E11.5	8.16	24	2.94	7.68

### ***Hematopoietic clusters arise from distinct hemogenic endothelial clones***

I next determined whether distinct hemogenic endothelial clones that existed in the endothelial layer<sup>58,59</sup> could account for IAHC formation and could be partially responsible for the expansion of their cell number. I initially crossed a constitutive VE-cadherin-Cre to the R26r-mTmG reporter line (VECAD/mTmG) (Figure 6A-E). I found that recombination in this line resulted in the excision of mTomato (mTom) and expression of mGFP in endothelial cells (CD31<sup>+</sup>CD117<sup>-</sup>) and their hematopoietic (CD31<sup>+</sup>CD117<sup>+</sup>) derivatives, including IAHCs within the embryo (Figure S6A). Upon quantification, I found mGFP<sup>+</sup> labeling in ~ 75% of endothelial cells (CD31<sup>+</sup>CD117<sup>-</sup>) and ~50% of IAHCs (CD31<sup>+</sup>CD117<sup>+</sup>) (Fig. S6, A-B). Immunofluorescence also revealed mosaic expression of mGFP and Tomato in the endothelial cells and IAHCs in the DA (Fig. S6C-D). Interestingly, 39% of IAHCs contained both mGFP<sup>+</sup> and mTom<sup>+</sup> cells (Fig. S6E). About 53% of the total IAHCs examined (n=57) were mGFP<sup>+</sup> only, while 9% of IAHCs were not Cre recombined and hence, mTom<sup>+</sup> only (Fig. S6E). Together, these data indicate that distinct HE clones may contribute to the formation of IAHCs. To test this hypothesis, I performed low dose clonal labeling using Cdh5(PAC)-CreERT crossed to R26r-mTmG reporter line (iCdh5/mTmG) (Fig. S6F-H). I administered a range of low dose tamoxifen (50 -150 µg) to pregnant females at E8.5, prior to any IAHC formation, to label only endothelial clones and IAHCs. I then determined the percent recombination in endothelial cells and IAHCs (Fig. S6F-H). The analysis revealed that a dose of 100 µg allowed for ~10% labeling of the dorsal aorta (ECs and IAHCs). I then administered the optimal clonal labelling dose of 100 µg (0.1mg) at E8.5 and analyzed the clonal labelling of IAHCs at E10.5 (Figure 6A). Outcomes of the experiment were identified as IAHCs from a single

origin (mGFP<sup>+</sup>only), polyclonal origin (mGFP<sup>+</sup>/mTom<sup>+</sup>) or unlabeled (no Cre recombination (mTom<sup>+</sup>only) (Figure 6B). Following induction, I observed mosaic mGFP<sup>+</sup> and mTom<sup>+</sup> labeling in the endothelium and IAHCs of the DA (Figure 6C). For the analysis of clonality, I excluded mTom<sup>+</sup> only IAHCs because I cannot conclude whether these IAHCs arose from a single clone since no Cre recombination/fate tracing took place. I evaluated 190 IAHCs (n=5 embryos) and noted 44 IAHCs at E10.5 were either monoclonal (mGFP<sup>+</sup>) or polyclonal (mGFP<sup>+</sup>/mTom<sup>+</sup>). Quantification of single color (mGFP<sup>+</sup> only) and mosaic IAHCs (mGFP<sup>+</sup> Tom<sup>+</sup>) at E10.5 revealed that the majority of IAHCs (39 out of 44) were mosaic (Figure 6E), while only 6 out of 44 IAHCs were from a mGFP<sup>+</sup> only clone. I further extended this analysis to IAHCs at E11.5. I evaluated 54 IAHCs and found 11 IAHCs to be either monoclonal (mGFP<sup>+</sup>) or polyclonal (mGFP<sup>+</sup>/mTom<sup>+</sup>), Table 2. At this time point, I observed a similar trend as at E10.5 where a majority of IAHCs were mosaic (8 out of 11) and minority derived from a single mGFP<sup>+</sup> clone (3 out of 11) (Figure 6F). To further support these observations, I also utilized the confetti reporter system by crossing inducible Cre animals with the confetti reporter animals (Figure 7A). Outcomes of this cross yield random recombination and labeling of endothelial cells and their hematopoietic derivatives that can be identified with four distinct fluorescent labels: mCFP, RFP, YFP and GFP (Figure 7B). In terms of inferring clonality, single color IAHCs denote monoclonal origin and multi-color IAHCs denote polyclonal origin (Figure 7C). One caveat of this line is that high amounts (1.5 – 2 mg) of tamoxifen needed to be administered prior to IAHC formation (E7.5 and/or E8.5) as recombination levels are low (not shown). Administration of these levels of tamoxifen do not appear to be detrimental to embryonic development (Figure 7D, E). Upon immunofluorescence,

IAHCs are indeed labeled with the confetti reporter system (Figure 7F). However, the frequency of GFP labeled cells (not shown) were low relative to the frequency of CFP, RFP and YFP labelled cells (Figure 7F). The low percentage of recombination observed within this line may be due the inefficiency of the Cdh5-Cre or perhaps that the cell cycle length of these IAHCs is too short for the accumulation of the fluorescent protein after recombination. Nonetheless, quantification of labeled IAHCs (n=4) at E10.5 showed that IAHCs contained cells that were labeled with two distinct fluorescent colors (Figure 7F, G). Collectively, these data further support that IAHCs largely derive from a polyclonal origin.

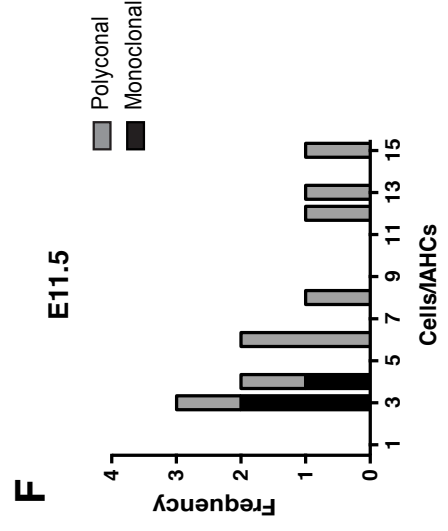
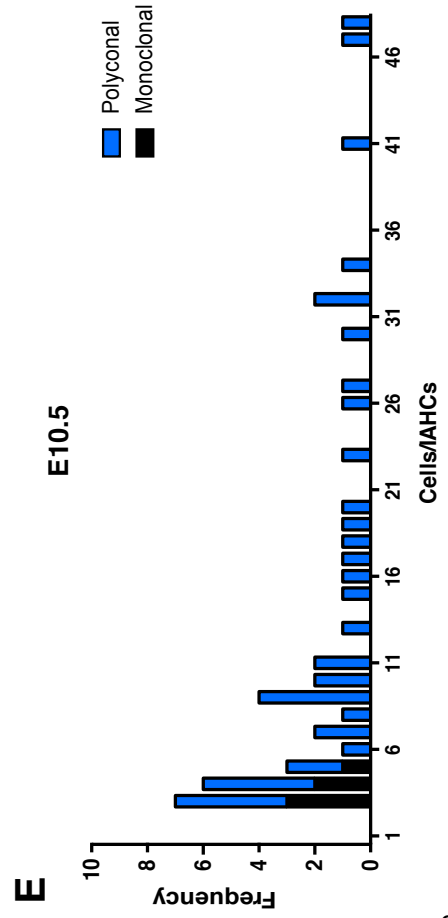
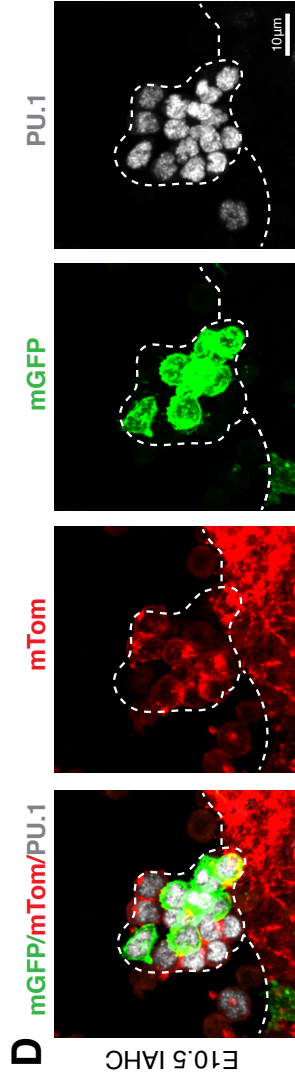
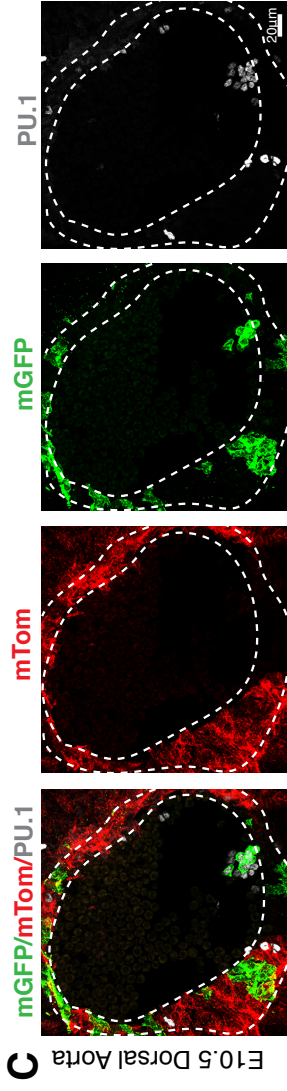
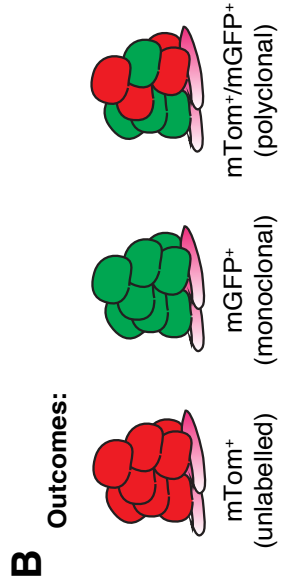
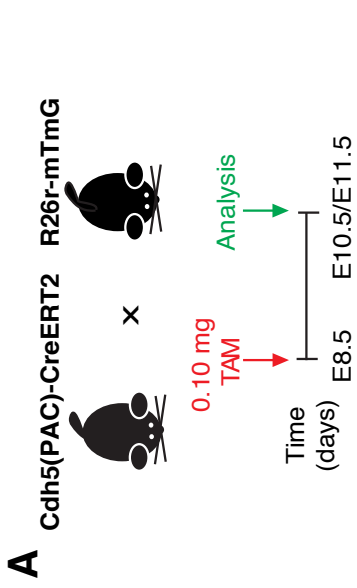


**Figure 6. Low dose clonal labeling of IAHCs reveal polyclonal origin of IAHCs**

(A) Experimental schema: *Cdh5*(PAC)-CreERT2 animals were crossed with R26<sup>r</sup>-mTmG lines. Pregnant females were induced with a low dose of tamoxifen (0.1mg) at E8.5 prior to IAHC formation. Embryos evaluated at E10.5 and E11.5. (B) Potential outcomes following low dose induction: unlabeled (no Cre recombination, mTom<sup>+</sup> only, monoclonal (mGFP<sup>+</sup> only) and polyclonal (mGFP<sup>+</sup>mTom<sup>+</sup>)). (C) Fluorescence of the dorsal aorta (DA) at E10.5 (broken lines) after low dose induction shows mosaic mGFP<sup>+</sup> (green) expression in a background of mTom<sup>+</sup> (red) cells. PU.1 (grey) labels an IAHC. Scale bar, 20  $\mu$ m. (D) Higher magnification of the IAHC depicted in (C) which is noted to contain both mGFP<sup>+</sup> (green) and mTom<sup>+</sup> (red) cells. PU.1 (grey) labels cells in the IAHC and some single hematopoietic cells. Scale bar, 10  $\mu$ m. (E) Analysis of IAHC clonality at E10.5. Monoclonal (mGFP<sup>+</sup> only) IAHCs denoted by black bars, and polyclonal (mGFP<sup>+</sup>mTom<sup>+</sup>) IAHCs denoted by blue bars. A total of 190 IAHCs were analyzed. n=2-3 litters. (F) Analysis of IAHC clonality at E11.5. Monoclonal (mGFP<sup>+</sup> only) IAHCs denoted by black bars, and polyclonal (mGFP<sup>+</sup>mTom<sup>+</sup>) IAHCs denoted by grey bars. A total of 57 IAHCs were analyzed, n=2-3 litters.

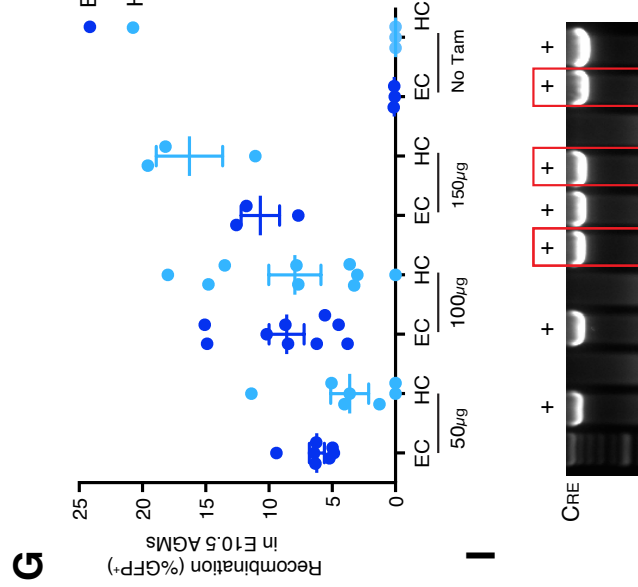
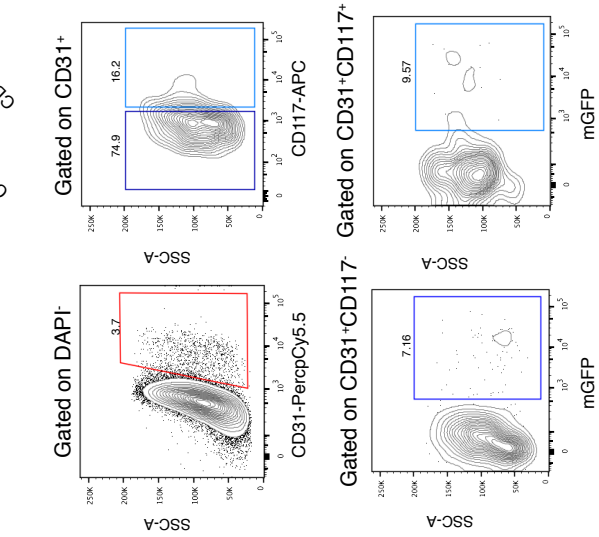
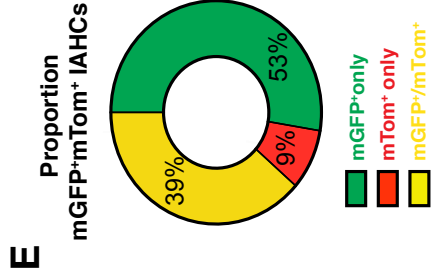
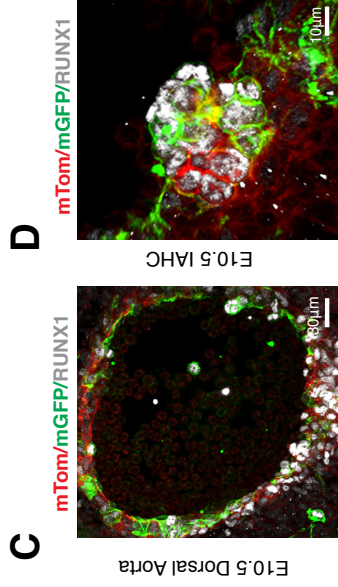
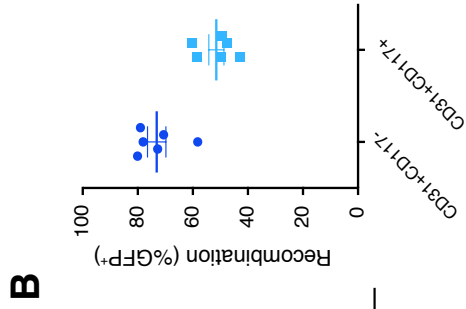
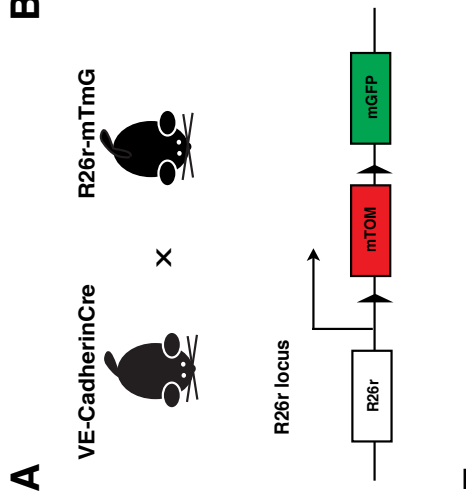


### Figure 6 – Supplement. Tamoxifen Dose Finding Experiments

- (A) Constitutive VE-Cadherin Cre (VECAD-Cre) animals were crossed to a R26r mTmG reporter mouse (mTmG).
- (B) 75% recombination levels were achieved in the CD31<sup>+</sup>CD117GFP<sup>+</sup> endothelial cell population, and 55% in CD31<sup>+</sup>CD117<sup>+</sup>mGFP<sup>+</sup> IAHC population. n=3 litters.
- (C) Fluorescence imaging of dorsal aorta from a constitutive VECAD-Cre/mTmG embryo demonstrates cells containing mGFP<sup>+</sup> (green) and mTom<sup>+</sup> (red), Runx1 immunofluorescence in grey. Scale bar 30  $\mu$ m.
- (D) An IAHC from a constitutive VECAD-Cre/mTmG embryo depicts a cluster containing both mGFP<sup>+</sup> and mTom<sup>+</sup> cells. Runx1 marks IAHCs (grey). Scale bar 10  $\mu$ m.
- (E) Quantification of IAHCs shows that 53% exhibit mGFP<sup>+</sup> only, 39% both mTom<sup>+</sup> and mGFP<sup>+</sup> and 9% mTom<sup>+</sup> only IAHCs. (Green, mGFP<sup>+</sup> only; Red mTom<sup>+</sup> only; Yellow mGFP<sup>+</sup> and mTom<sup>+</sup>) n=3 litters, 57 IAHCs scored.
- (F) Gating strategy of mGFP<sup>+</sup> IAHCs and mGFP<sup>+</sup> ECs. IAHC population was gated on as DAPI<sup>-</sup>/SSEA1<sup>-</sup>CD31<sup>+</sup>CD117<sup>+</sup> cells and EC population was gated on as DAPI<sup>-</sup>/SSEA1<sup>-</sup>CD31<sup>+</sup>CD117<sup>-</sup> cells.
- (G) Recombination in E10.5 AGMs after dosing experiment which ranged from 0.05 to 0.1 mg of tamoxifen. 0.1 mg of tamoxifen was selected as the optimal dose based on <10% of recombination in the endothelial (dark blue circles) and IAHC (light blue circles) population. No tamoxifen control shows 0% recombination.
- (H) Genotypes of E10.5 embryos for Cre transgene. Red boxes were the Cre<sup>+</sup> samples but were not induced with tamoxifen in (G).

**Table 2. Total IAHCs evaluated for clonality at E10.5 and E11.5**

<b>Age</b>	<b>Total IAHCs Evaluated</b>	<b>Total Scored</b>	<b>Total Unlabeled</b>
E10.5 (n=5)	190	44 (23%)	146(77%)
E11.5 (n=3)	57	11(19%)	46(81%)

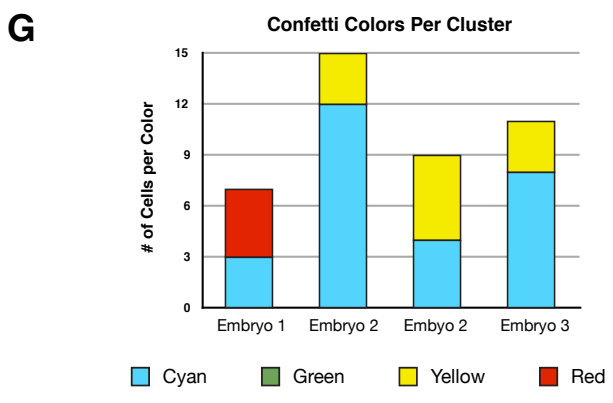
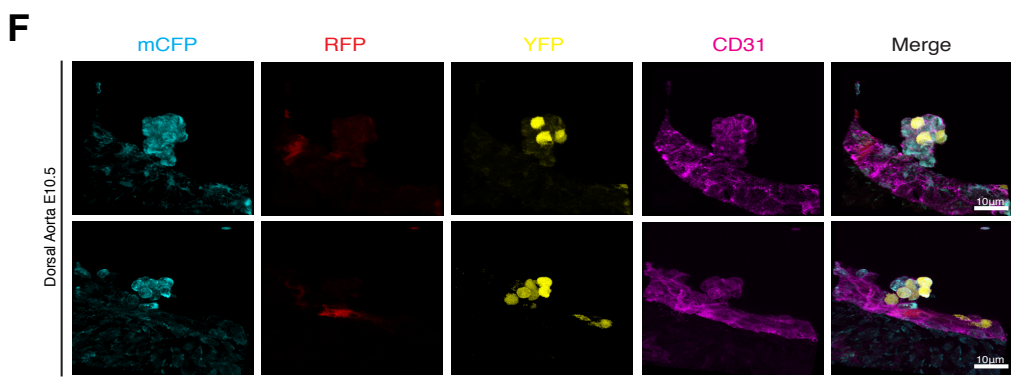
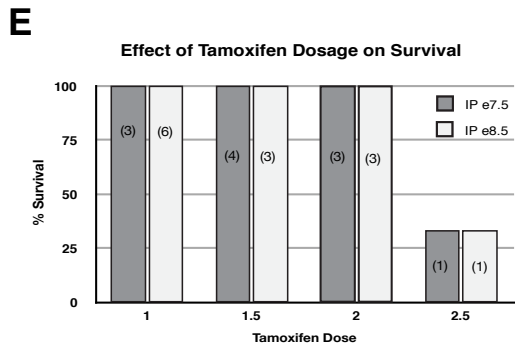
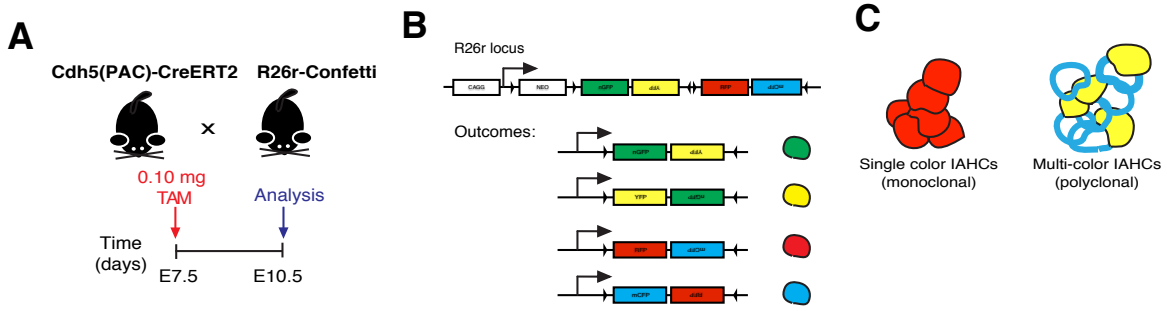


**Figure 7. Polyclonality of IAHCs is supported using the Cdh5Cre-confetti reporter system.**

(A) Inducible Cdh5Cre animals were crossed with confetti reporter animals. (B) Outcomes of the recombination could be identified by four fluorescent labels: GFP, YFP, CFP, and RFP. (C) Clonality outcomes are identified as monoclonal if IAHCs are of single-color and polyclonal if IAHCs are of multi-color. (D) Embryos that were given high doses (1.5 mg and 2.0 mg) of tamoxifen at E8.5 show no detectable defects at E10.5. Scale bars are 0.5 millimeters. (E) Quantification of survival after induction of high dose of tamoxifen at E7.5 and E8.5 shows no lethality until 2.5 mg of tamoxifen are administered. (F) Immunofluorescence of Cdh5-confetti labeled IAHCs shows cells labeled with CFP, YFP and RFP. CD31 (purple) was used as a marker of endothelial cells and hematopoietic clusters. (G) Quantification of Cdh5-confetti labeled IAHCs from different embryos reveal polyclonal origins of IAHCs. Scale bars are 10  $\mu$ m.

## Discussion

Live imaging is a powerful technique that has allowed the visualization of IAHCs in the context of their near-native environment<sup>26,60</sup>. My initial observations depicted that indeed the ventral endothelium of the dorsal aorta contained hemogenic endothelial cells that emerge and adapt a rounded morphology (Figure 2A) which resembled that of a blood cell, akin to what has been described as EHT using zebrafish imaging<sup>36</sup>. Interestingly, in subsequent live imaging experiments using labeled lines such as VE-cadherinCre-tdTomato, labeled cells appeared to extend different types of cellular protrusions which resemble filopodia or a narrow cytoplasmic bridge (Figure 2B). In the visualization of IAHCs using Cdh5-mTmG reporter, I observed cell division within IAHCs (Figure 3). These newly formed cells resided in the uppermost part of the right IAHC (Figure 3). Interestingly, a labeled cell appeared to extend a protrusion to these newly formed cells (Figure 3). This extension was followed by what appeared to be a fragmentation of either the cell itself or its membrane protrusion as some cell structures remained attached to the newly formed cells (Figure 3). The appearance of this filopodial extension and the fragmentation behavior observed in these videos are reminiscent of megakaryocyte proplatelet formation<sup>61</sup>. During this process, megakaryocytes extend branch-like processes called proplatelets which function as a linear assembly for platelets. Proplatelets are organized in tandem and are inter-connected by cytoplasmic bridges. Megakaryocytes release these proplatelets which then fragment into platelets. Overall, the data suggest that megakaryocytes may play a role in supporting IAHC and HSC development in the AGM. Megakaryocytes appear in the yolk sac at E7.5<sup>62</sup> and could

reach the AGM upon the initiation of circulation at E8.5. Furthermore, megakaryocytes have been reported to support HSCs in the bone marrow by regulating their quiescence<sup>63,64</sup>.

While I was unable to capture the processes that lead to IAHC cluster formation from a single hemogenic endothelial cell, I was able to visualize the dynamic behavior of pre-formed IAHCs. The results of these initial experiments revealed the ability of IAHCs to interact with each other and with other cells in the dorsal aorta. Interestingly, cells from IAHCs do not appear to “break” from their cluster formation suggesting that there may be a mechanism that allows for the maintenance of a single cluster. From these observations, I speculate that a cluster may be acting as a transitory niche and that interactions between the cells within an IAHC or with other cells in proximity may have important implications for the specification and maturation of IAHCs into HSCs.

In this chapter, I have also uncovered the rapid cell divisions that succeed the process of endothelial-to-hematopoietic transition. Specifically, I found that the total length of the cell cycle of IAHCs at E10.5 is approximately 5 hours which allows for a single clone to theoretically give rise to up to 23 cells within a 24-hour time period between E9.5 to E10.5. To reconcile these findings with observations that depict IAHCs having  $\geq 23$  cells, I discovered the presence of distinct clones within the endothelium that contribute to IAHC formation. Collectively, these data suggest that following EHT, IAHC formation is succeeded by rapid cell divisions from distinct clones that may serve to prevent clonal exhaustion and promote heterogeneity. Indeed, observations from clonal labeling experiments performed in zebrafish suggest the existence of up to 30 clones per

aorta during active the hemogenic window. <sup>59</sup>. In addition, rapid cell divisions may establish an initial pool of pre-HSCs from which HSCs mature from by E11.5. Correspondingly, the cell cycle length of E11.5 IAHCs lengthen to about 8 hours. This observation is intriguing as fetal liver (FL) HSCs have been estimated to have a mean generation time of 10.6 hours <sup>65</sup>. Thus, the lengthening of cell cycle from E10.5 to E11.5 may be commiserate with the E11.5 IAHC repopulation ability.

## **CHAPTER 2:**

**Intra-aortic hematopoietic clusters contain cells that are positioned at different phases of the cell cycle and have varying engraftment potential during the early and late stages of the hemogenic window**

## Introduction

The cell cycle activity of hematopoietic stem cells (HSCs) throughout the lifetime of the organism is dynamic and is linked to their ability to self-renew and to differentiate<sup>66</sup>. IAHCs from the AGM are thought to mature into HSCs with low proliferation<sup>42</sup> and the kinetics of their cell cycle remain largely unknown. Fetal-HSCs rapidly proliferate and differentiate in the fetal liver with generation times of within 10-14 hours<sup>65,67</sup>. Adult HSCs, in contrary, reside in the bone marrow and remain mostly quiescent<sup>68-71</sup>. Together, fetal<sup>65</sup> and adult HSCs<sup>67</sup> appear to transit at slower rates relative to their more differentiated progenitor counterparts which display generation times of within 5-6 hours<sup>65</sup>. Furthermore, a prolonged cell cycle length due to a prolonged G1 passage appear to be a characteristic of both fetal and adult HSCs<sup>65,72,73</sup>.

The progression of HSCs through the cell cycle both *in vitro* and *in vivo*<sup>65,67,74-77</sup> is accompanied by notable changes in their engraftment potential. Several lines of evidence suggest that cell cycle position may influence repopulation activity<sup>75-77</sup>. Indeed, fetal HSCs in the G<sub>0</sub>/G1 appear to engraft adult recipients better than their S/G2/M counterparts<sup>65</sup>. Whether embryonic HSCs contained in IAHCs display similar cell cycle features as to those of FL and BM HSCs remain to be clarified. In this chapter, I tested whether HSCs from ontogeny are at a specific cell cycle phase and whether their cell cycle phase influences their engraftment into the adult BM.

## Materials and Methods

### *Mice*

Mouse lines used for these experiments were Fucci Green [Tg(CAG mAG/GMNN)504Amiy] and Fucci Red [Tg(CAG-mKO2/CDT1)596Amiy]<sup>78</sup>. Mice were housed under a barrier facility following IACUC procedures and animal protocols were conducted under the University of California San Francisco Laboratory Guidelines.

### *Genotyping*

#### *FUCCI PCR Program*

94°C x 5 min. with HotStart, 94°C x 1 min., 55°C x 30s, 72°C x 2 min. repeat for 31 cycles, 72°C x 10 min., and hold at 4°C infinitely.

### *Primers*

Primer stock concentrations were prepared at 100 µM. A 10x dilution is performed to prepare working concentrations of 10 µM. Primers were stored in -20°C.

Name	Forward Primer	Reverse Primer
Fucci - Green	5'-CTT-CTT-CTA-CGA-CAT-CAG-GTT-3'	5'-GCA-TCT-AGA-TTA-CAG-CGC-CTT-TCT-CCG-TTT-TTC-TGC-3'
Fucci- Red	5'-ATG-ACA-CTA-CGC-GTC-ACA-AT-3'	5'-GCA-TCT-AGA-TTA-TTC-CTT-TAT-CTT-CTG-GCC-CGG-AGA-3'

### *Immunofluorescence*

E10.5 - E11.5 Fucci embryos were fixed in 4% paraformaldehyde (PFA) solution at room temperature for 20 minutes or in 2% PFA overnight. Samples were frozen in Tissue-Tek OCT Compound (Sakura Finetek, 4583). 20-30 µm cryosections were obtained (Thermo Scientific Micron, HM550). Slides were incubated in blocking buffer (PBS, 0.5% Triton-X100) with 5% serum for 1hr. Primary antibodies for CD31 were incubated at 4°C

overnight or room temperature for 2 hours in blocking buffer. Slides were washed (PBS 0.05% Tween), incubated with the secondary antibody for 1 hour, stained with 2g/μl DAPI and mounted in Vectamount (Vector Laboratories, H-5000). Images were captured on a Leica SPE Confocal Microscope.

### ***Flow Cytometry***

Whole embryos were screened for Fucci positivity under a benchtop fluorescence microscope. Subsequently selected AGMs were dissociated as previously described (Lizama et al. 2014) and stained for 30 min at 4°C with agitation. Single cell suspensions were sorted in a BD FACS Aria III. Flow cytometric analyses were performed on a FACS Verse or FACS Aria III with FACSDiva 8.0 software (BD Biosciences) and data analyzed using FlowJo v10.0.7 (Tree Star). Antibodies were purchased from BD Biosciences: CD117-APC (#553356), CD31-Percp Cy5.5 (#562861), V450-SSEA-1 (#561561). Isotype controls used were: IgG2b-APC (#55391), IgM-V450 (#560861), IgG1-PercpCy5.5 (#562861). Cells were sorted using a FACS Aria III cell sorter.

### ***Bone Marrow Transplantation***

8-12 week old CD45.2 C57Bl/6 FUCCI mice were used as donors for cell isolation. E10-E10.5 (30-39sp) and E11-E11.5 (40-48sp) AGMs were sorted for SSEA-1<sup>-</sup>/CD31<sup>+</sup>/CD117<sup>+</sup> FUCCI-Red or FUCCI-Green as donor cells. 8-12 week old CD45.1 C57Bl/6-Boy/J wild type mice were used as recipients for cell transplantation. Congenic recipient mice (CD45.1) were irradiated with 900 rads, split dose, 3 hours apart using a cesium source. Purified donor cells were injected intravenously with 200,000 spleen helper cells, and hematopoietic reconstitution was monitored over time in the peripheral blood based on CD45.2 expression. Recipients with ≥1% donor chimerism were

considered reconstituted. Transplanted mice were kept on antibiotic-containing food for 2 weeks. Recipients of helper cells and congenic donor cells were used as negative control, and recipients of  $4 \times 10^6$  CD45.2 whole bone marrow cells were used as positive control. All mice were maintained at UCSF in accordance with IACUC approved protocols.

## Results

### *IAHCs during development are positioned at different phases of the cell cycle as the hemogenic window progresses*

In Chapter 1, the findings that a higher proportion of IAHCs were mainly in the S-phase at E10.5 versus E11.5 together with the increase in the average cell cycle length (Figure 5 G-I) prompted me to evaluate whether the position of IAHCs in the cell cycle might be different during the two time points of the hemogenic window. To test this, I utilized the FUCCI (Fluorescence Ubiquitin Cell Cycle Indicator) reporter mouse line. In this line, CDT1-mKusabiraOrange2 (mKO2) marks cells in G1 and GEMININ-AzamiGreen (mAG) marks cells in S/G2/M (Figure 8A). I first verified the expression of these markers relative to DAPI incorporation (Figure S8A) to determine if the fluorescently labelled cells with either mKO2-CDT1 and/or mAG-GEMININ corresponds to appropriate cell cycle stage by DNA content. I then evaluated expression of these markers in the developing neural tube and AGM (Figure S8B-C), and confirmed the pattern of G1 (FUCCI-Red) versus S/G2/M (FUCCI-Green) in the neural tube. In this region, the somites are labelled with FUCCI-Red denoting that cells are in G1, while the rest of cells in the neural tube are labeled with FUCCI-Green indicating that they are in the S-phase. I also examined immunofluorescence of the protein GEMININ, in the context of the transgenic reporter FUCCI-Green (GEMININ-AzamiGreen (mAG)) within the developing endothelium and IAHCs (Figure 8D). I found that the mAG reporter tended to underreport (by 12%) cells that express GEMININ (Figure S8E). With that in mind, I evaluated IAHCs for their expression of FUCCI-Green and FUCCI-Red, and noted that cells which make up a single

IAHC are positioned in different cell cycle phases. Thus, the cells comprising one IAHC were not necessarily synchronized in their cell cycles (Figure 8B). To analyze the IAHC population as a whole, I used FACS to discern the cell cycle phase of IAHCs at E10.5 (pre-HSC stage) and E11.5 (definitive-HSC). FACS analysis revealed that at E10.5, ~2% of the SSEA-1<sup>-</sup>CD31<sup>+</sup>CD117<sup>+</sup> IAHC population (IAHCs) resided in G1, while ~28% resided in the S/G2/M (Figure 8C, D). Interestingly, at E11.5 ~35% of the IAHC population now resided in G1, and ~11% resided in S/G2/M (Figure 8C, D). Overall, the data suggest that there is a shift in the cell cycle position of IAHC cells as the hemogenic window progresses during development. This previously unappreciated difference between the cell cycle position of IAHC cells at E10.5 and E11.5 has led me to postulate whether the cell cycle position may influence repopulation potential.

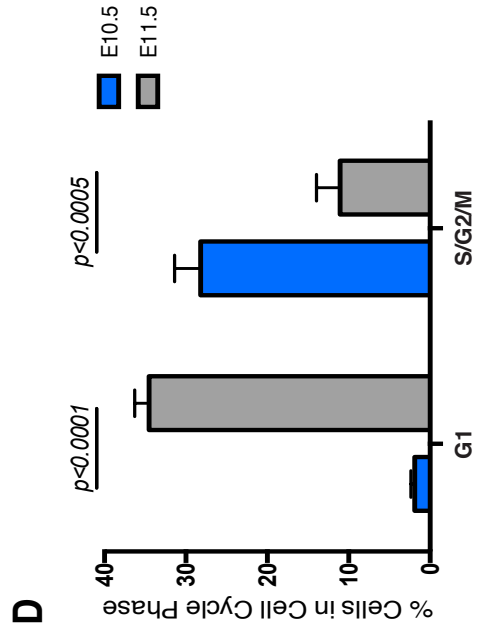
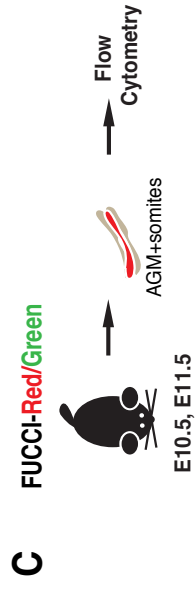
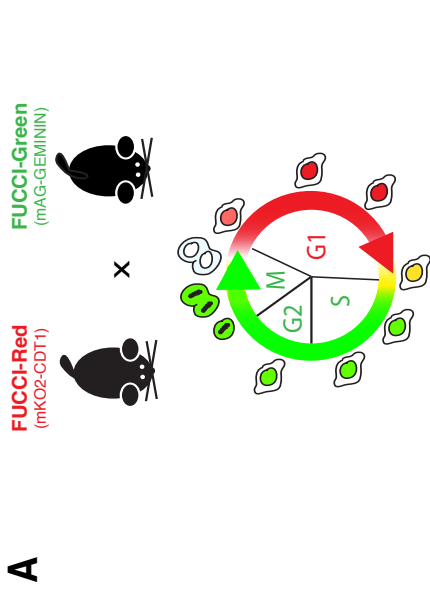
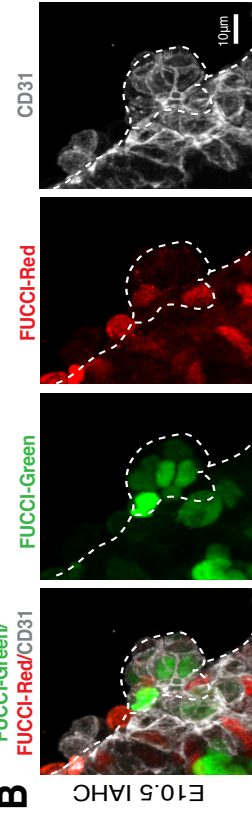
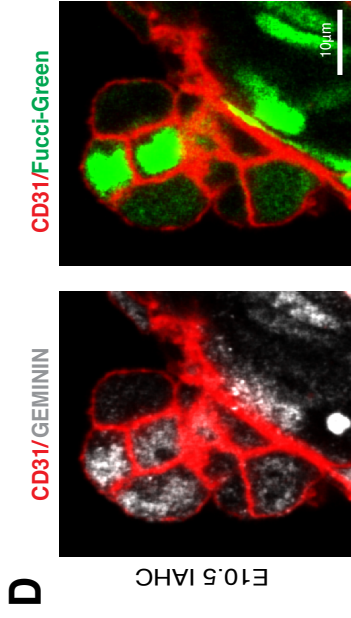
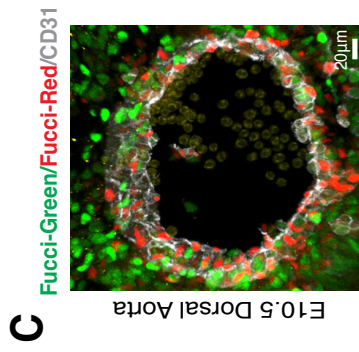
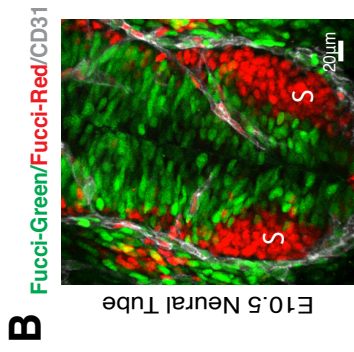
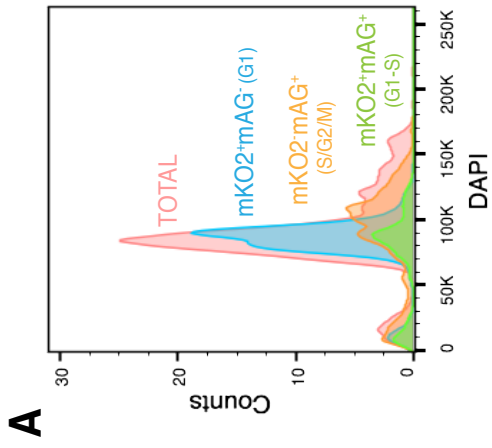


**Figure 8. IAHCs are positioned at different phase of the cell cycle during E10.5 and E11.5.**

- (A) FUCCI-Red (mKO2-CDT1) were crossed with FUCCI-Green (mAG-GEMININ) animals. In G1, GEMININ is degraded and active CDT1 tagged with Kusabira Orange (mKO2) is present thereby marking cells in G1. Similarly, in S/G2/M, CDT1 is degraded and GEMININ tagged with Azami Green (mAG) is active thus labeling cells in S/G2/M.
- (B) Immunofluorescence of an IAHC at E10.5 shows cells in G1 labelled by mKO2 (red) and cells in S/G2/M (green) labelled by mAG. Broken lines depict the IAHC. CD31 (grey) marks the endothelium. Scale bar, 10  $\mu$ m.
- (C) FUCCI AGMs at E10.5 and E11.5 were analyzed by flow cytometry for cell populations in G1 and S/G2/M by their respective fluorescence mKO (red) and mAG (green).
- (D) Comparison of IAHC populations (DAPI<sup>-</sup>SSEA1<sup>+</sup>CD31<sup>+</sup>CD117<sup>+</sup>) in G1 and S/G2/M at E10.5 (blue bars) and E11.5 (grey bars). The data demonstrate that at E10.5 the majority of IAHC cells are in S/G2/M vs. G1 (28.2% S/G2/M vs. 1.92% G1, t-test with Welch's correction  $p < 0.0001$ ), while at E11.5, majority of the IAHC cells are G1 v. S/G2/M (11% S/G2/M vs. 34.5% G1, t-test with Welch's correction  $p < 0.0005$ ). n=4, All data shown as mean +/- SEM.



**E**

Total Cells (n= 6 IAHCs)	Geminin+FucciGreen+	Geminin+FucciGreen-
42	60%	12%

**Figure 8- Supplement. Validation of the FUCCI system.**

(A) Validation of the FUCCI line against DNA content marker, DAPI, shows that FUCCI distinguishes cells that are G1 and S/G2/M phases of the cell cycle per DAPI histogram. (B) FUCCI labeling in the developing neural tube shows localization of FUCCI-Red<sup>+</sup> G1 cells (red) in the somite and Fucci-Green<sup>+</sup> S/G2/M cells (green) in the middle/central cavity of the neural tube. S denotes somite. CD31 in grey. Scale bar, 20  $\mu$ m. (C) FUCCI labeling of the dorsal aorta identifies cells that are in G1 (Fucci-Red<sup>+</sup>) and S/G2/M (Fucci-Green<sup>+</sup>). CD31 is used to denote the endothelium (grey). Scale bar, 20  $\mu$ m. (D) An image of an IAHc containing Fucci-Green<sup>+</sup> (green) cells which overlap with the staining of S/G2/M marker, geminin (grey). Scale bar, 10  $\mu$ m. (E) Quantification of Fucci-Green<sup>+</sup> and GEMININ<sup>+</sup> shows that ~12% of GEMININ<sup>+</sup> cells have weak or undetectable levels of mAG (green) fluorescence

### ***Cell cycle phase does not fully account for repopulation activity***

Previous studies from Nygren and colleagues which examined the cell cycle kinetics of E14.5 fetal-liver HSCs (FL-HSCs) found that a prolonged cell cycle length is a characteristic of HSCs<sup>65</sup>. In line with these observations, the data I gathered so far demonstrate a prolongation of the cell cycle length at E11.5 which is coincident with the observed repopulation activity during this time point. To determine whether cell cycle position may influence the behavior of IAHC cells in a reconstitution assay, I directly transplanted irradiated adult animals with FACS sorted SSEA-1<sup>-</sup>CD31<sup>+</sup>CD117<sup>+</sup>mKO2<sup>+</sup> cells (G1 IAHCs) and SSEA-1<sup>-</sup>CD31<sup>+</sup>CD117<sup>+</sup>mAG<sup>+</sup> cells (S/G2/M IAHCs) from E10.5 and E11.5 AGMs (Figure 9A). I found that regardless of their phase in the cell cycle, E10.5 IAHCs (n=8-9 per group) had undetectable levels of chimerism even after 16 weeks post-transplantation (Figure 9B, C). Conversely, only E11.5 IAHCs showed engraftment ( $\geq 1\%$  donor-derived cells) within 8 weeks and 16 weeks. Yet, some animals demonstrated only transient levels of engraftment (Figure 9B). Of the E11.5 transplanted animals (n=12 each group) we determined to have been repopulated by 8 weeks (1 each in of the G1 and S/G2/M groups respectively), only one had stable engraftment by 16 weeks as measured by peripheral blood chimerism (Figure 9B). In the 16-week engraftment cohort, the animal transplanted with G1 IAHCs (fuschia triangle) demonstrated stable repopulation while the animal transplanted with S/G2/M IAHCs (blue hexagon) did not appear to maintain the  $>1\%$  level of engraftment long. However, I did detect a low level of chimerism ( $>16$  weeks) in 1 animal that received S/G2/M IAHCs (Figure 9B, G1 IAHCs 14.5% vs S/G2/M IAHCs 0.3%, Table 3). Further evaluation of lineage markers for B and T cells, as well as myeloid lineage cells within these animals, revealed that these cells were indeed able to

reconstitute the different hematopoietic cell lineages (Figure 9D). Overall, the data suggest that E10.5 IAHCs do not contain an engraftable HSC population, regardless of enrichment for cells either in G1 or S/G2/M. However, these data also support that E11.5 IAHCs contain adult engraftable HSCs that may be enriched in the G1 (versus S/G2/M) cell cycle phase, similar to their fetal and adult HSC counterparts<sup>65,74,77,79</sup>.

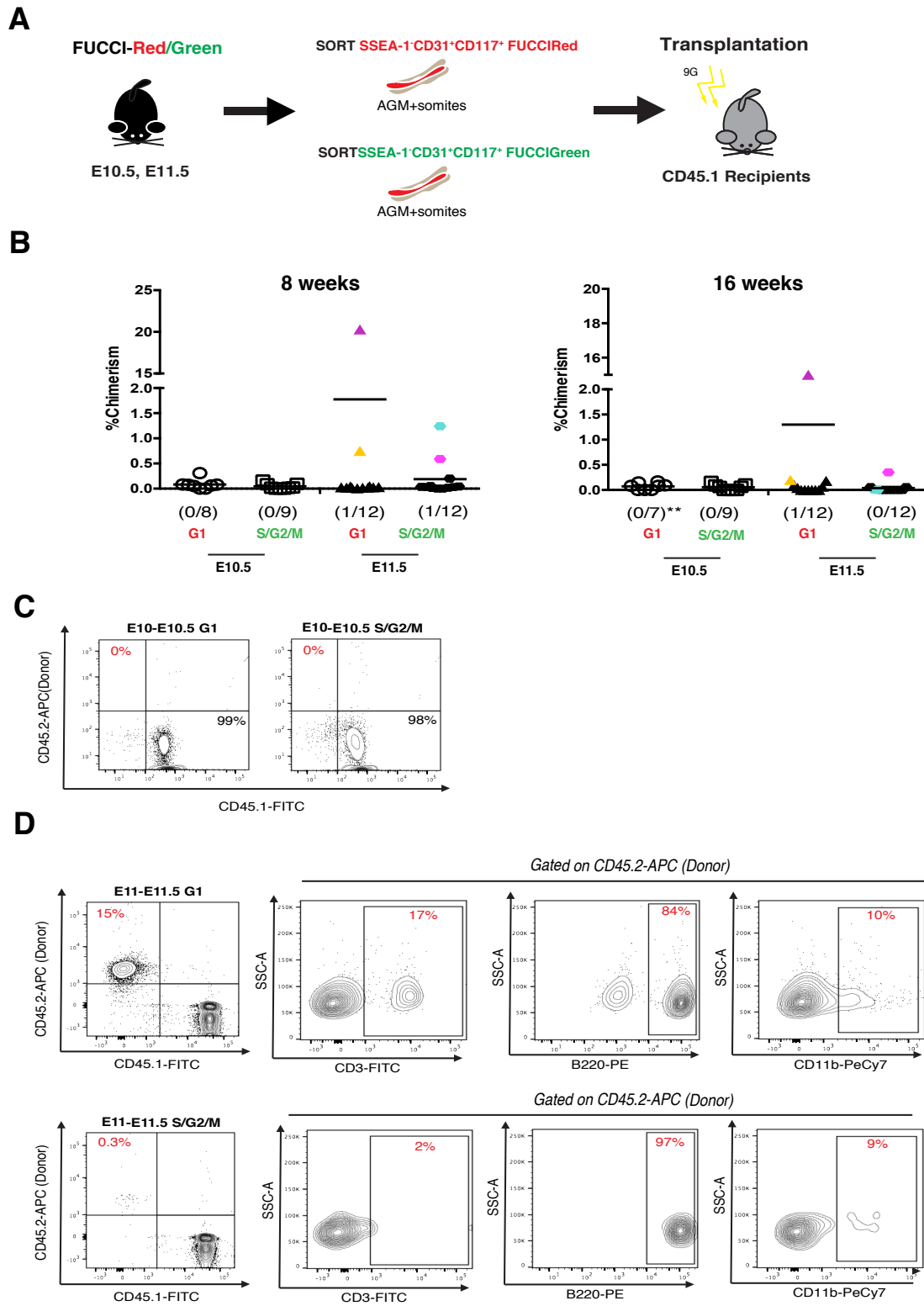


### Figure 9. Direct transplantation of E10.5 and E11.5 Fucci labeled IAHCs.

(A) Transplantation experimental scheme. IAHC cell populations (DAPI<sup>-</sup>SSEA1<sup>-</sup>CD31<sup>+</sup>CD117<sup>+</sup>) from Fucci-Red (mKO2-CDT1) and Fucci-Green (mAG-GEMININ) mice were sorted (cell number = 200- 2000 cells per group) and directly transplanted into irradiated adult recipients (E10.5 n = 8-9 per group, E11.5 n=12 per group). (B) Analysis of engraftment (defined as >1% peripheral blood chimerism) at 8 and 16 weeks depicts E10.5 Fucci-Red (open circles) and green (open squares) IAHCs with no detectable engraftment (0/8 and 0/9 respectively). E11.5 Fucci-Red (triangles) and Fucci-green (hexagons) each exhibit one animal with detectable levels of engraftment (1/12 and 1/12 respectively) at 8 weeks (each labelled with a separate color). Only the recipient of G1 IAHCs retains stable engraftment at 16 weeks (fuchsia triangle). No stable engraftment was seen in E11.5 Fucci-Green at 16 weeks, although there was low level of chimerism detected (0.3%) (fuchsia hexagon). Double asterisks indicates the occurrence of mortality in the cohort. (C) Representative FACS plots of E10.5 Fucci-Red and Fucci-Green IAHCs show no detectable engraftment by 16 weeks. (D) FACS plots of E11.5 G1 IAHCs (fuchsia triangle) demonstrate 15% donor reconstitution and peripheral blood contribution to the T (CD3-FITC), B (B220-PE) and myeloid (CD11b-PeCy7) lineages by 16 weeks and for E11.5 S/G2/M (blue hexagon) 0.3% donor engraftment and lineage contribution to B, T, and myeloid lineages.

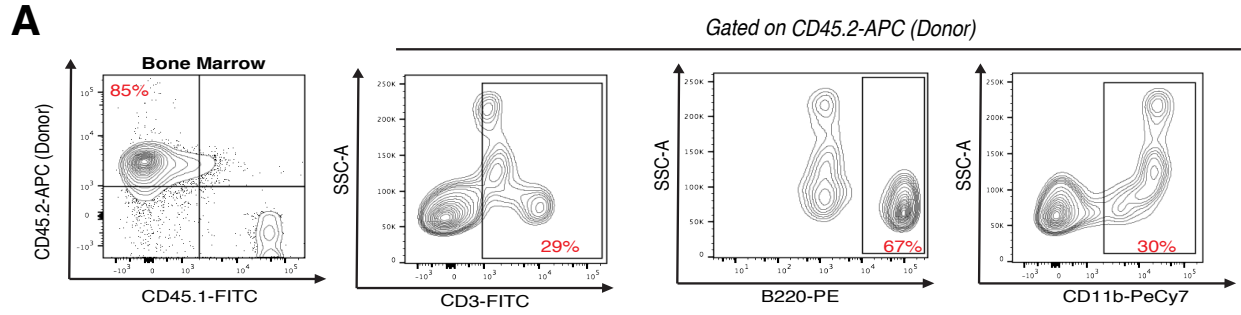


**Figure 9 – Supplement. Transplantation of donor bone marrow cells as positive control.**

(A) 4 million bone marrow cells from CD45.2 donor mice were transplanted into CD45.1 irradiated hosts. Analysis of peripheral blood at 16 weeks reveal 85% donor reconstitution and differentiation into CD3+ T cells, B220+ B cells and C11b+ myeloid cells.

**Table 3. Transplantation cell number and engraftment.**

<b>Sample Name</b>	<b>Cell Number</b>	<b>% CD45.2 Donor Cells (8 weeks)</b>	<b>Engraftment (1%)</b>	<b>% CD45.2 Donor Cells (16 weeks)</b>	<b>Engraftment (1%)</b>
Fucci Red e10-e10.5	700	0.000%	N	0.000%	N
Fucci Red e10-e10.5	346	0.000%	N	0.000%	N
Fucci Red e10-e10.5	681	0.052%	N	MORTALITY	
Fucci Red e10-e10.5	490	0.063%	N	0.082%	N
Fucci Red e10-e10.5	476	0.082%	N	0.170%	N
Fucci Red e10-e10.5	902	0.310%	N	0.095%	N
Fucci Red e10-e10.5	1095	0.077%	N	0.150%	N
Fucci Red e10-e10.5	332	0.081%	N	0%	N
		<b>TOTAL</b>	<b>0/8</b>	<b>TOTAL**</b>	<b>0/7</b>
Fucci Green e10-e10.5	639	0.018%	N	0.000%	N
Fucci Green e10-e10.5	100	0.000%	N	0.000%	N
Fucci Green e10-e10.5	650	0.018%	N	0.000%	N
Fucci Green e10-e10.5	729	0.000%	N	0.160%	N
Fucci Green e10-e10.5	1597	0.024%	N	0.064%	N
Fucci Green e10-e10.5	1152	0.097%	N	0.091%	N
Fucci Green e10-e10.5	504	0.000%	N	0.110%	N
Fucci Green e10-e10.5	1298	0.087%	N	0.059%	N
Fucci Green e10-e10.5	446	0.160%	N	0%	N
		<b>TOTAL</b>	<b>0/9</b>	<b>TOTAL</b>	<b>0/9</b>

<b>Sample Name</b>	<b>Cell Number</b>	<b>% CD45.2 Donor Cells (8 weeks)</b>	<b>Engraftment (1%)</b>	<b>% CD45.2 Donor Cells (16 weeks)</b>	<b>Engraftment (1%)</b>
Fucci Red e11-e11.5	716	0.017%	N	0.000%	N
Fucci Red e11-e11.5	1194	20.300%	Y	14.900%	Y
Fucci Red e11-e11.5	1111	0.026%	N	0.000%	N
Fucci Red e11-e11.5	600	0.750%	N	0.200%	N
Fucci Red e11-e11.5	1397	0.044%	N	0.040%	N
Fucci Red e11-e11.5	750	0.048%	N	0.066%	N
Fucci Red e11-e11.5	1591.5	0.006%	N	0.002%	N
Fucci Red e11-e11.5	1591.5	0.021%	N	0.100%	N
Fucci Red e11-e11.5	1890	0.015%	N	0.000%	N
Fucci Red e11-e11.5	200	0.031%	N	0.000%	N
Fucci Red e11-e11.5	1180	0.019%	N	0.180%	N
		<b>TOTAL</b>	<b>1/12</b>	<b>TOTAL</b>	<b>1/12</b>
Fucci Green e11-e11.5	300	0.018%	N	0.000%	N
Fucci Green e11-e11.5	558	0.044%	N	0.000%	N
Fucci Green e11-e11.5	1,164	0.590%	N	0.350%	N
Fucci Green e11-e11.5	414	0.053%	N	0.000%	N
Fucci Green e11-e11.5	814	1.240%	Y	0.006%	N
Fucci Green e11-e11.5	1000	0.200%	N	0.056%	N
Fucci Green e11-e11.5	674	0.031%	N	0.000%	N
Fucci Green e11-e11.5	600	0.000%	N	0.057%	N

<b>Sample Name</b>	<b>Cell Number</b>	<b>% CD45.2 Donor Cells (8 weeks)</b>	<b>Engraftment (1%)</b>	<b>% CD45.2 Donor Cells (16 weeks)</b>	<b>Engraftment (1%)</b>
Fucci Green e11-e11.5	1600	0.000%	N	0.000%	N
Fucci Green e11-e11.5	650	0.032%	N	0.000%	N
Fucci Green e11-e11.5	200	0.034%	N	0.000%	N
Fucci Green e11-e11.5	2011	0.014%	N	0.000%	N
		<b>TOTAL</b>	<b>1/12</b>	<b>TOTAL</b>	<b>0/12</b>

## Discussion

In this chapter, I uncovered that IAHCs between E10.5 and E11.5 are positioned at different phases of the cell cycle. IAHCs at E10.5 appeared to contain more cells in the S/G2/M phases of the cell cycle than in G1 (Figure 8D). Intriguingly, by E11.5, IAHCs appeared to contain more cells in G1 than in S/G2/M (Figure 8D). This data together with the findings that the cell cycle lengthens by E11.5 (Figure 5I) suggest that the G1 phase of cell cycle likely undergoes a prolongation step. Overall, these findings imply that the maturation process leading to the emergence of definitive HSCs by E11.5 may include a lengthening of the cell cycle.

In this chapter, I also investigated whether position in the cell cycle of IAHCs affects their engraftment in the adult BM. The number of IAHCs detected during the hemogenic window is small with only ~ 1500 – 2000 cells in an E10.5 AGM. The average percentage of cells that exhibit either FUCCI-Green or FUCCI-Red fluorescence ranges from 600 to 700 at E10.5, and 800 to 1000 cells at E11.5 per AGM. Thus, a significant limitation of the transplantation study is that only a limited number of cells could be harvested from any single litter for transplantation. As low as ~200 cells and as much ~2000 cells per adult mouse were transplanted, and these results may be at the detection boundary of the assay. Nonetheless, these findings highlight that adjusting for cell cycle phase at E10.5 (by selection and transplantation of the minority G1 population) does not overcome the inability of these cells to engraft adult hosts. Interestingly, the data demonstrate that E11.5 IAHCs harbor definitive HSCs that may be enriched in the G1 phase of the cell

cycle. The data also support that definitive HSCs in the S/G2/M contained in E11.5 IAHCs may also possess some engraftment potential albeit lower than their G1 counterpart. Collectively, the lengthening of cell cycle from E10.5 to E11.5 and the coincident ability of E11.5 IAHCs to engraft adult irradiated recipients point that the cell cycle itself may influence HSC maturation and engraftment potential.

### **Chapter 3:**

**Transcriptional profiling of intra-aortic hematopoietic cluster populations across developmental age and cell cycle phase reveals a potential role for complement genes in the maturation of HSPCs**

## Introduction

Recent advances in RNA sequencing have given researchers the opportunity to analyze whole transcriptomes of different cell types allowing for the characterization of distinct functional states. Global transcriptional profiles of adult hematopoietic stem cells from single cells have been extensively analyzed and have revealed clonal heterogeneity even amongst cells from homogeneous populations<sup>80,81</sup>. Furthermore, evidence also suggest that the cell cycle state of adult HSCs is a major source of transcriptional variation and may be linked with aging<sup>82</sup>.

Transcriptional profiling of HSCs from ontogeny, however, revealed distinct transcriptional profiles yet with a commonality with macrophages<sup>83</sup>. Currently, it remains unclear how these distinct transcriptional profiles relate to their functionality and whether embryonic HSCs display a cell cycle-specific programming. The data I have collected so far further support that the cell cycle phase may influence the engraftment of HSCs contained in E11.5 IAHCs. To further uncover any potential link between developmental age, cell cycle state, and adult engraftment potential, I transcriptionally profiled IAHCs in G1 and S/G2/M from E10.5 and E11.5. In this chapter, I describe the changes in the transcriptional landscape of IAHCs across their developmental age and their cell cycle stage, and implicate a potential role for complement in the maturation of IAHCs and their engraftment in the adult irradiated bone marrow.

## **Materials and Methods**

### ***RNA Isolation and Sequencing***

Samples were pooled from 2-3 liter embryos from FUCCI crosses (See Chapter 2, Methods). Total RNA was isolated and purified from sorted cells using the QIAGEN RNeasy Plus Micro Kit (#74034) following manufacturer's instructions. RNA integrity was determined using a Bioanalyzer. Samples were ribo-depleted and amplified with Ovation RNA-Seq System V2. Paired-end 2 x 100 bp sequencing was performed using the Illumina HiSeq2000 machine. RNA sequencing analysis was done using Galaxy (<https://usegalaxy.org/u/laiumiunix/w/rnaseqjoandata>) with a False discovery rate (FDR) of 0.085. Raw data files were deposited to the NCBI Gene Expression Omnibus (GEO) with GEO accession number, GSE93314. Transcripts with  $\geq 2$ -fold change expression were further analyzed using the Ingenuity Pathway Analysis to identify key biological functions and pathways that are expected to be more active in E11.5 than E10.5. To be more stringent, we focused our analysis to functions and pathways with a positive z-score.

### ***QPCR RNA Isolation and cDNA transformation***

SSEA-1<sup>-</sup>/CD31<sup>+</sup>/CD117<sup>+</sup> IAHC cell populations were sorted from wild-type E10.5 and E11.5 embryos. RNA was isolated using QIAGEN RNeasy Plus Micro Kit (#74034) and concentrations were determined using a Nanodrop and Agilent 2100 Bioanalyzer with an RNA Pico Chip. 40 – 50  $\mu$ g of RNA was transformed to cDNA using the Superscript VILO Mastermix (Thermofisher, #11755050). cDNA was diluted to give a final concentration of 0.5 ng/ $\mu$ l. Samples were run on BioRad 384-well thermocycler.

### ***cDNA Transformation Program***

25°C x 10 min, 42°C x 1 hour, 30 min, 85°C x 5 min and hold at 4°C indefinitely.

### **QPCR Program**

95°C x 10 min, 95°C x 30s, 60°C x 1 min, repeat 39x and perform the melt curve program:

95°C x 30s, 60°C x 1 min, 60°C x 15s, 93.6°C/0.7°C.

### **QPCR Primers**

Name	Forward Primer	Reverse Primer
C1QA	5'-ACA-AGG-TCC-TCA-CCA-ACC-AG-3'	5'-AAG-ATG-CTG-TCG-GCT-TCA-GT-3'
C1QB	5'-TCT-AGG-GAC-CCA-GAC-TTC-CG 3'	5'-CAG-GGG-CTT-CCT-GTG-TAT-GG-3'
C1QC	5'-AGT-GCC-CCT-CTA-CTA-CT-3'	5'-CGG-GAA-ACA-GTA-GGA-AAC-CA-3'
CD93	5'-AAA-CGC-TGT-GTG-TCC-CTC-AT-3'	5'-TGC-TGT-TAC-CTG-GAG-CTT-CG-3'
C3AR	5'-TGA-CAG-GTC-AGC-TCC-TTC-CT-3'	5'-CAT-TAG-GAG-GCT-TTC-CAC-CA-3'
GAPDH	5'-TGT-GTC-CGT-CGT-GGA-TCT-GA-3'	5'-CCT-GCT-TCA-CCA-CCT-TCT-TGA-3'
RPL3RT	5'-GAT-GAG-TGT-AAA-AGG-CGC-TTC-3'	5'-CTT-GGT-GAA-AGC-CTT-CTT-CTT-3'

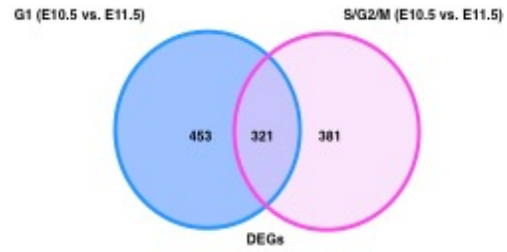
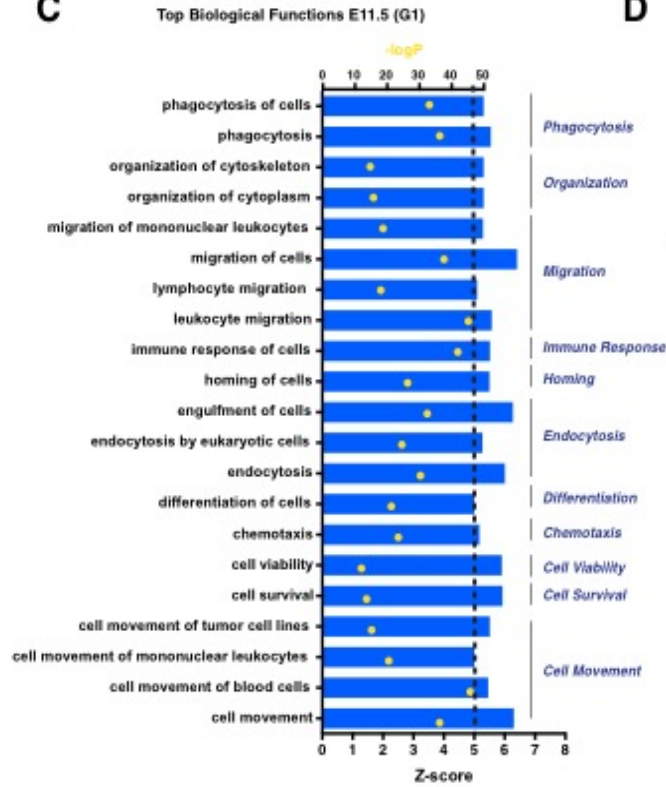
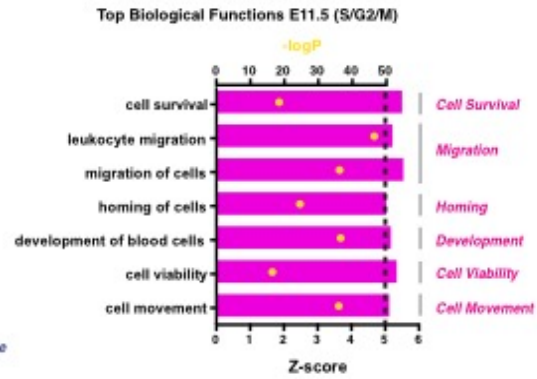
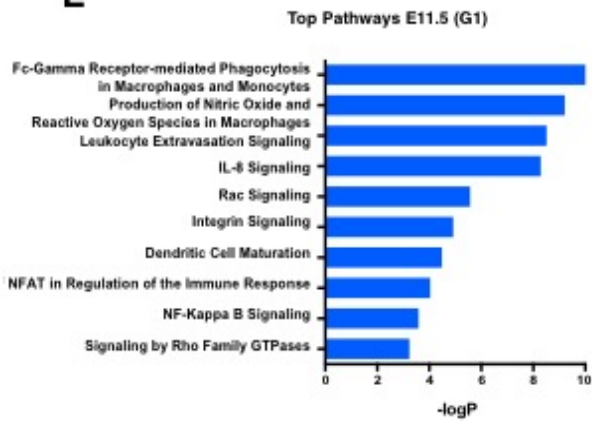
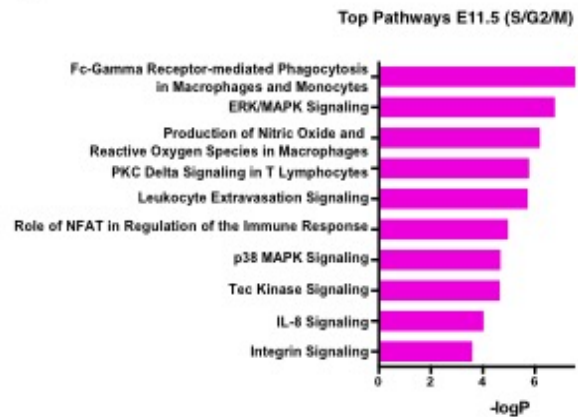
## Results

### ***Cell cycle-specific transcriptional profiling of E10.5 and E11.5 IAHCs reveal transcriptional programs related to cell movement and cell migration***

To further define transcriptional differences that underlie the developmental age and maturation of IAHCs, I performed RNA sequencing on four samples: E10.5 and E11.5 SSEA-1<sup>-</sup>CD31<sup>+</sup>CD117<sup>+</sup>mKO2<sup>+</sup> (G1 IAHCs) and E10.5 and E11.5 SSEA-1<sup>-</sup>CD31<sup>+</sup>CD117<sup>+</sup>mAG<sup>+</sup> (S/G2/M IAHCs) (Figure 10A). I have identified a total of 774 genes for G1 and 703 genes for S/G2/M that were differentially expressed between E10.5 and E11.5. G1 contained 453 unique genes and similarly, S/G2/M contained 381 unique genes (Figure 10B). To determine the molecular signature of IAHCs that change according to developmental age, only genes with a 2-fold change in expression were analyzed using the Ingenuity Pathway Analysis (IPA, Ingenuity Systems, [www.ingenuity.com](http://www.ingenuity.com)). I used two metrics, the p-value and the activation z-score, to identify the most important downstream effects related to age. A positive z-score indicates an increased functional or pathway activity in E11.5 relative E10.5 for both G1 and S/G2/M samples. The p-value, calculated with Fisher's exact test, indicates the likelihood that the association between a set of genes in our data set and a biological function or pathway is significant.

The analysis revealed that genes overexpressed in E11.5 versus E10.5 at G1, regulated 11 top functions related to a variety of cellular processes (Figure 10C). Interestingly, the functions that were significantly increased were those that were involved in *cell migration, endocytosis, cell movement, phagocytosis, cell organization, immune*

*response, homing differentiation and cell survival.* Perhaps not surprising was that the analysis of genes overexpressed in E11.5 versus E10.5 at S/G2/M, yielded 6 top functions similar to those in G1 with *cell migration, cell movement, homing, cell survival,* and *development* being significantly activated (Figure 10D). Furthermore, examination of top canonical pathways in G1 revealed activation of signaling pathways that regulated *phagocytosis, nitric oxide signaling, leukocyte extravasation* and *IL-8* (Figure 10E). The analysis of canonical pathways in S/G2/M showed activation of *phagocytosis, ERK signaling, nitric oxide signaling* and *PKC Delta signaling* (Figure 10F). Overall, the data suggest that regardless of the cell cycle phase, cell movement and cell migration programs are established in IAHCs by E11.5.

**A****B****C****D****E****F**

## Figure 10. Transcriptional profile of E10.5 and E11.5 FUCCI labeled IAHCs.

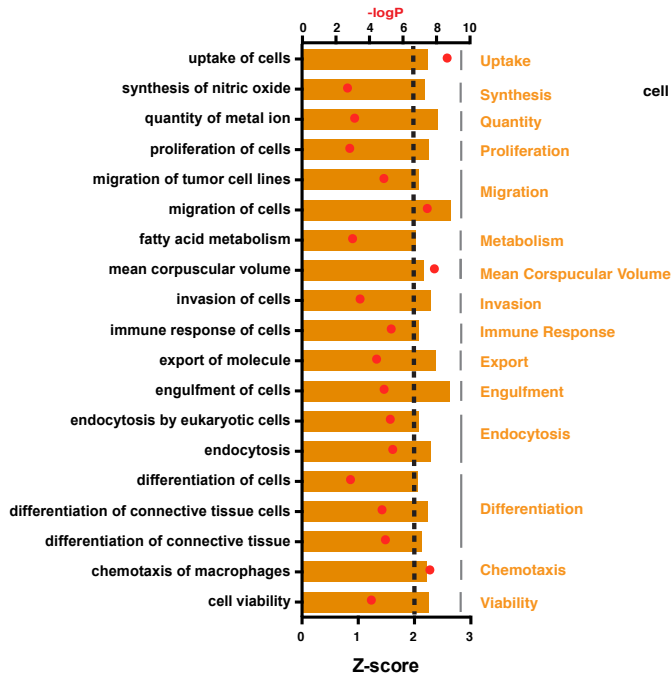
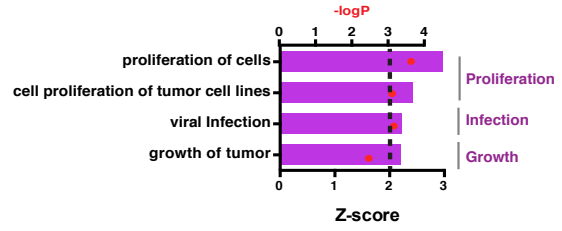
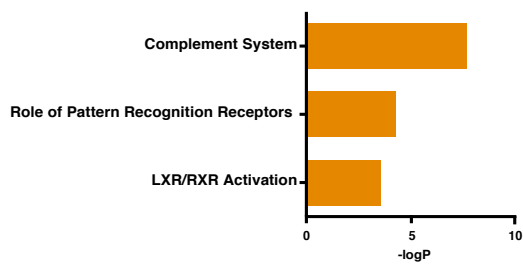
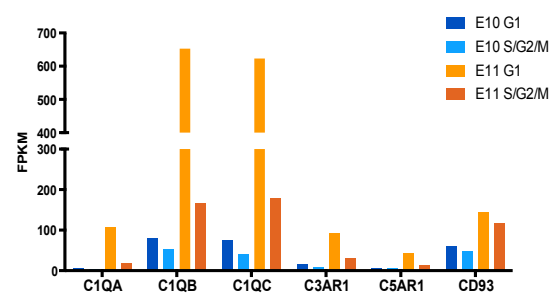
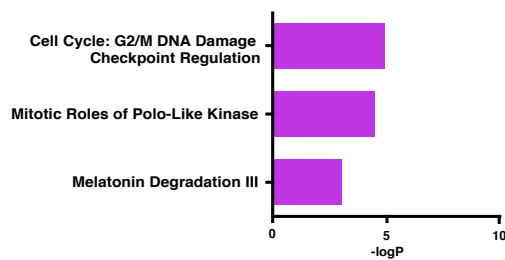
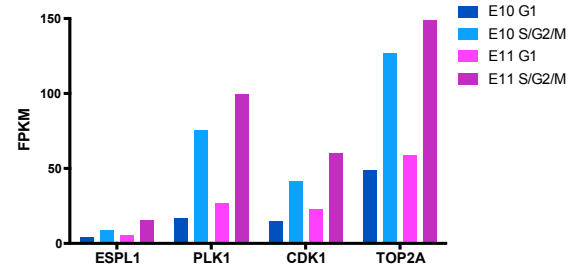
(A) RNA sequencing experimental scheme. IAHC cell populations (DAPI<sup>+</sup>SSEA1<sup>-</sup>CD31<sup>+</sup>CD117<sup>+</sup>) from FUCCI-Red (mKO2-CDT1) and FUCCI-Green (mAG-GEMININ) mice were sorted and subjected to RNA sequencing. (cell number, n = 300 – 8000 cells pooled from 2-3 liters per group per age). (B) Venn diagram depicts the number of common and unique genes between G1 (FUCCI-Red) and S/G2/M (FUCCI-Green) IAHCs. 453 unique genes were upregulated in G1 E11.5 IAHCs vs. G1 E10.5 IAHCs. Similarly, 381 unique genes were upregulated in S/G2/M E11.5 IAHCs vs. S/G2/M E10.5 IAHCs. These 2 groups share 321 common genes. (C) The RNASeq analysis of top biological functions (z-score >5, p<0.05) enriched in E11.5 IAHCs at G1 relative to E10.5 IAHCs at G1 identifies the top 11 increased biological functions involved a variety of cellular processes including: *phagocytosis, organization, migration, immune response, homing, endocytosis, differentiation, chemotaxis, cell viability, cell survival and cell movement*. z-score  $\geq 5$  (black dotted line), p-value (yellow dots) via Fisher's exact test. (D) The RNASeq analysis of top biological functions (z-score  $\geq 5$ , p<0.05) enriched in E11.5 IAHCs at S/G2/M relative to E10.5 at S/G2/M reveals the top 6 increased biological functions that are involved in: *cell survival, migration, homing, development, cell viability and cell movement*. Not surprisingly, these categories are similar to those in E11.5 IAHCs at G1. z-score  $\geq 5$  (black dotted line), p-value (yellow dots) via Fisher's exact test. (E) The analysis of canonical pathways (z-score  $\geq 5$ , p<0.05) that are active in E11.5 IAHCs at G1 compared to E10.5 IAHCs at G1 identifies the top 10 activated signaling pathways which include: *Gamma receptor-mediated phagocytosis, production of NO, leukocyte extravasation, IL-8 signaling, Rac signaling, integrin signaling, dendritic cell maturation, NFAT signaling, NF-Kappa B signaling and Rho GTPase signaling*. (F) The analysis of canonical pathways (z-score  $\geq 5$ , p<0.05) that are active in E11.5 IAHCs at S/G2/M compared to E10.5 IAHCs at S/G2/M identifies the top 10 activated signaling pathways which include: *Gamma receptor-mediated phagocytosis, ERK/MAPK signaling, production of NO, PKC delta signaling, leukocyte extravasation, NFAT signaling, p38 MAPK signaling, Tec Kinase signaling, IL-8 signaling and integrin signaling*.

### ***Molecular differences between E11.5 G1 and S/G2/M IAHCs point to complement activation for a role in engraftment***

Since the transplantation data suggest that both E11.5 G1 and S/G2/M IAHCs contain HSCs with different engraftment potential, I next determined the molecular differences related to the cell cycle that may influence engraftment. I identified 106 differentially expressed genes between G1 and S/G2/M IAHCs. First, I compared transcripts from E11.5 S/G2/M with E11.5 G1 to identify functions that were upregulated within the G1 phase of the cell cycle. Surprisingly, genes overexpressed in G1 regulated 14 main functions that were involved in different cellular processes. The biological functions that were most significantly activated include *chemotaxis, migration, uptake* and *cell volume* (Figure 11A). As expected, comparison of E11.5 G1 with E11.5 S/G2/M transcripts to identify functions upregulated within the S/G2/M phases of the cell cycle yielded functions relating to *proliferation, infection* and *growth* (Figure 11B) with *proliferation* being the most significantly activated.

The analysis of upregulated pathways in E11.5 G1 versus S/G2/M also revealed activation of canonical signaling pathways that regulated the *complement system, roles of pattern recognition receptors* and *LXR/RXR activation* (Figure 11C). Indeed, several complement genes such as receptors C5AR, C3AR and complement components C1QA, C1QB, and C1QC were activated in G1 (Figure 11D). In contrast, examination of transcripts upregulated in S/G2/M revealed activation of signaling pathways regulating the *G2/M DNA damage checkpoint, mitotic roles polo-like kinases* and *melatonin*

*degradation* (Figure 11E). Subsequently, I observed activation of ESPL1, PLK1, CDK1 and TOP2A transcripts associated with the S/G2/M phases of the cell cycle (Figure 11F). Overall, when comparing between age groups, I find the activation of complement genes in E11.5 G1 IAHCs suggesting that this may be a critical pathway for the maturation of pre-HSCs to definitive HSCs resulting in adult engraftment. To further corroborate these results, since there appears to be a higher expression of complement-related genes at E11.5 versus E10.5, I sorted wild-type E10.5 and E11.5 SSEA-1<sup>-</sup>/CD31<sup>+</sup>/CD117<sup>+</sup> IAHC cell populations for QPCR validation. Indeed, C1Q subcomponents as well its complement C1 receptor, CD93 were significantly increased at E11.5 relative to E10.5 (Figure 12A). Together, these suggests that activation of complement genes may play a role in HSPC maturation.

**A****Top Function G1 (E11.5)****B****Top Function S/G2/M (E11.5)****C****Pathways Upregulated in G1 (E11.5)****D****E****Pathways Upregulated in S/G2/M (E11.5)****F**

**Figure 11. Molecular differences between E11.5 G1 IAHCs and E11.5 S/G2/M IAHCs.**

(A) Analysis of top biological functions ( $z > 0$ ,  $p < 0.05$ ) enriched in E11.5 G1 IAHCs relative to E11.5 S/G2/M IAHCs reveal the top 15 upregulated functions in G1 which include: *uptake, synthesis, quantity, proliferation, migration, metabolism, corpuscular volume, invasion, immune response, export, engulfment, endocytosis, differentiation, chemotaxis and viability*. z-score black dotted line, p-value red dots. (B) Analysis of top biological functions ( $z > 0$ ,  $p < 0.05$ ) enriched in E11.5 S/G2/M IAHCs relative to E11.5 G1 IAHCs reveal the top 3 functions increased in S/G2/M which are: *proliferation, infection and growth*. z-score black dotted line, p-value red dots. (C) The canonical signaling pathways that are activated ( $z > 0$ ,  $p < 0.05$ ) in E11.5 G1 IAHCs compared to E11.5 S/G2/M IAHCs include: *complement system, pattern recognition receptors, LXR/RXR activation*. (D) Complement transcripts are increased in E11.5 G1 IAHCs relative to E11.5 S/G2/M IAHCs. FPKM, Fragments Per Kilobase of transcript per Million. (E) The canonical signaling pathways that are activated ( $z > 0$ ,  $p < 0.05$ ) in E11.5 S/G2/M IAHCs compared to E11.5 G1 IAHCs include: *G2/M DNA damage checkpoint, mitotic roles for polo-like kinases and melatonin degradation*. (F) Cell cycle related genes have increased activation during the S/G2/M phases of the cell cycle regardless of developmental age. FPKM, Fragments Per Kilobase of transcript per Million.

A

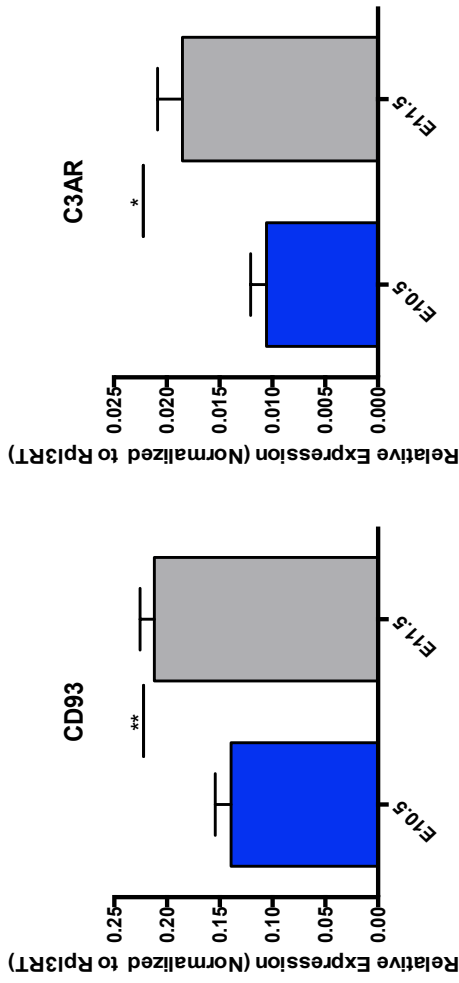
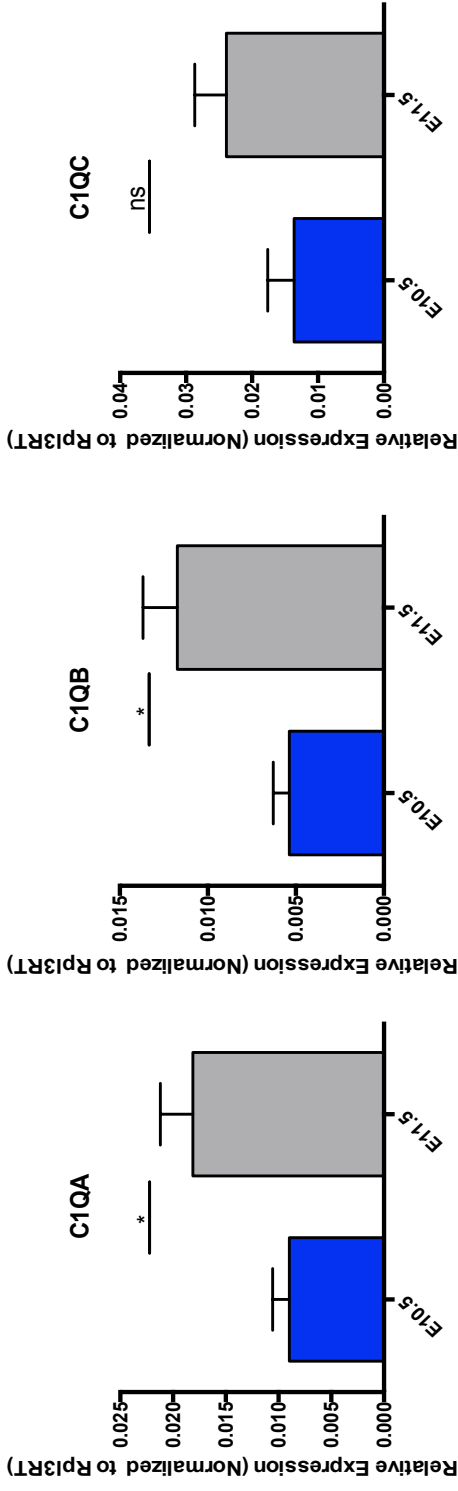


**Figure 12. QPCR validation of complement-related genes.**

(A) Genes related to C1Q subcomponent genes increase by E11.5. *C1QA* (\* $p \leq 0.0314$ ) and *C1QB* (\* $p \leq 0.021$ ), were significantly increased at E11.5 versus E10.5 while *C1QC* (NS = 0.1323) displayed an increasing trend. *CD93* (\*\* $p \leq 0.004$ ), the C1Q receptor and another complement receptor *C3AR* (\* $p \leq 0.02$ ) were also significantly increased by E11.5 versus E10.5.  $n=3$  liter each time point, Unpaired t-test with Welch's correction. Reads were normalized to housing keeping gene *Rpl3RT*.

## Discussion

In this chapter, transplantation of E11.5 G1 versus S/G2/M IAHCs suggested an advantage of G1 IAHCs to engraft irradiated adult recipients, albeit with low numbers than their S/G2/M counterpart. This observation is in line with earlier findings that HSCs in G1 have an engraftment advantage over HSCs in S/G2/M<sup>65,67</sup>. To further determine any link between developmental age, cell cycle phase and bone marrow engraftment, I performed RNA sequencing of IAHCs at E10.5 and E11.5 at different phases of the cell cycle. I found that IAHCs harbor a dynamic transcriptional landscape that changes with developmental age and cell cycle phase. In addition, I discovered that across developmental age by E11.5, an enrichment for genes that regulate “cell movement”, “migration” and “inflammatory response” become evident. These data further support the findings of McKinney-Freeman and colleagues that IAHCs may resemble a “macrophage-like signature”<sup>83</sup>; in addition to the recent wealth of information pointing to inflammatory signals being critical for early HSC development<sup>84-87</sup>. Furthermore, since it has been hypothesized that IAHCs migrate to the fetal liver after their formation in the AGM, it may be likely that the maturation process of E10.5 IAHCs may involve the activation of cell movement and cell migration signaling pathways that prepare IAHCs for entry into circulation. I further analyzed transcriptional profiles of E11.5 G1 IAHCs and I discovered an enrichment for transcripts that regulated the “immune response”, “chemotaxis” and “cell migration”. While not surprising, profiling of S/G2/M E11.5 IAHCs demonstrated an activation of signaling pathways that regulated “cell growth” and “proliferation”. Thus, these data suggest that during the G1 phase of the cell cycle, IAHCs may become

sensitive to a multitude of cellular cues which include immune and inflammatory signals that may regulate cell movement, egression into circulation, and consequently, migration towards the fetal liver.

There is evidence to suggest that complement activation plays a role in donor HSPC migration and homing post transplantation <sup>88-90</sup>. It has been shown that C1q enhances the responsiveness of HSPCs to the chemoattractant CXCL-12 (SDF-1) <sup>91</sup>. From the analysis of RNA sequencing, I found that genes of the classical complement cascade which include C1QA, C1QB and C1QC, as well as anaphylatoxin receptors, C3AR and C5AR, to be upregulated in E11.5 G1 IAHCs and have validated these observations with QPCR. Thus, these findings suggest that G1 IAHCs may be primed for homing to the adult bone marrow, and may explain the engraftment potential of G1 IAHCs relative to their S/G2/M counterparts.

## Discussion

Our understanding of the subsequent cellular processes following the emergence of hematopoietic stem and progenitor cells from the endothelium remains incomplete. For some time, the process leading to the existence of large IAHCs (>20 cells) in dorsal aorta has remained unclear. Furthermore, little is known about the maturation process from pre-HSC to HSC. The findings in this dissertation add to the field's current understanding of IAHC formation and pre-HSC to HSC maturation. In this work, I investigated the formation and expansion of HSPCs contained in the IAHCs of the dorsal aorta during the pre-HSC (E10.5) and HSC (E11.5) time-points of the hemogenic window. In summation, I found polyclonal origins of IAHCs with differing cell cycle kinetics, engraftment potential and transcriptional profiles.

In Chapter 1, I visualized cells in the dorsal aorta through live-imaging experiments. I observed the emergence of a rounded hematopoietic cell from the ventral floor as well as the appearance of different transient filopodial structures that resemble cytoplasmic bridges from megakaryocyte proplatelets. I also observed cell division in IAHCs and the extension of a filopodial structure towards the newly divided cells in the IAHC. The appearance of these structures has not been visualized until now and these data reveal dynamic behavior of the dorsal aortic endothelial cells and IAHCs. Furthermore, these data also support a potential role for megakaryocytes in IAHC formation and maturation, and HSC development.

In Chapter 1, I also characterized the cell cycle kinetics of IAHCs and determined

how IAHCs can be collectively be comprised of 20 cells and greater. First, I uncovered the rapid proliferation of IAHC cells following their transition into a hematopoietic fate from a hemogenic endothelial cell at E10.5. The 5-hour total generation time of IAHCs in part explains the wide range in cluster size observed at E10.5 and theoretically estimates that the maximum size of an IAHC from a single clone would be 23 cells. The data also show, for the first time, polyclonality of hematopoietic clusters as another contributor to IAHC size (cell number). A single hemogenic clone is unlikely to give rise to IAHCs with greater than 20 cells. Collectively, these findings support the formation of IAHCs from rather distinct hemogenic endothelial clones and implicate mosaicism of the hemogenic endothelium as a potential source of HSPC heterogeneity. Also in this chapter, I further uncovered that IAHCs from the two different hemogenic time points are positioned at different phases of the cell cycle and that the total generation time of IAHCs increases as the hemogenic window progresses towards an HSC time-point. These observations are in line with findings that support the prolongation of the cell cycle in fetal-liver (FL) HSCs as well as the differences in cell cycle position between FL-HSCs and FL-progenitors. Thus, it would appear that HSCs from any time point in development or adulthood share similarities in their cell cycle kinetics.

In Chapter 2, using the FUCCI reporter system, I show for the first time the influence of cell cycle phase of IAHCs on their adult engraftment potential. First, the data demonstrate that IAHCs from two different time-points of the hemogenic window are positioned at different phases of the cell cycle. A striking finding is that the IAHC population largely shifts from S/G2/M to the G1 phase of the cell cycle during the HSC

period of hemogenic window which is coincident with findings that FL-HSCs are largely in G1. It may be possible that IAHCs at E11.5 adopt similar characteristics as that of FL-HSCs before they enter circulation. Second, I directly tested whether the cell cycle phase of IAHCs influences their engraftment potential in the adult. Ultimately, I found that, regardless of their cell cycle phase, E10.5 IAHCs are unable to engraft adult irradiated recipients. Thus, this finding supports that E10.5 IAHCs contain immature pre-HSCs or progenitor cells. With regards to E11.5 IAHCs, the data show engraftment of adult irradiated recipients at low levels. When examined according to their cell cycle phase, E11.5 G1 IAHCs show engraftment whereas the S/G2/M counterpart does not. These data demonstrate that E11.5 IAHCs contain HSCs that may be enriched in the G1 phase of the cell cycle. Collectively, these findings so far suggest that maturation towards an HSC fate may include the lengthening of the cell cycle and the positioning of the cells in the G1 phase. These data also suggest that IAHCs may become sensitive to a variety of cellular/maturation cues when they are G1.

In Chapter 3, I discovered novel transcriptional profiles of IAHCs segmented by developmental age and cell cycle phase. The findings here show that across developmental age by E11.5, robust *cell migration* and *cell movement* transcriptional programs are established. These findings are not surprising as IAHCs enter circulation and migrate to the fetal liver by E11.5. When cell cycle phase is the only variable considered, E11.5 IAHCs show enrichment of complement genes suggesting that the complement pathway may play a role in the activation and migration of HSPCs. It would be interesting to determine which complement genes directly play a role in HSPC

activation and migration.

Finally, the findings in this thesis support a model following EHT where at E10.5, IAHCs form rapidly from the proliferation of distinct hemogenic clones (Figure 13). Subsequently, these IAHCs mature to HSPCs by E11.5, which include the prolongation of the cell cycle length and activation of a migratory and homing program which facilitate their transit into the fetal liver. These findings further lend credence to the establishment of a robust HSC program following EHT, such that the very properties (prolonged cell cycle length, engraftment in G0/G1, lengthening of G1) that define fetal liver and adult HSCs are reflected in the newly emerged embryonic AGM HSCs. Overall, the knowledge gained from this thesis work will enable studies that seek to further uncover the cellular and molecular processes of IAHC formation and pre-HSC to HSC maturation.

**A**

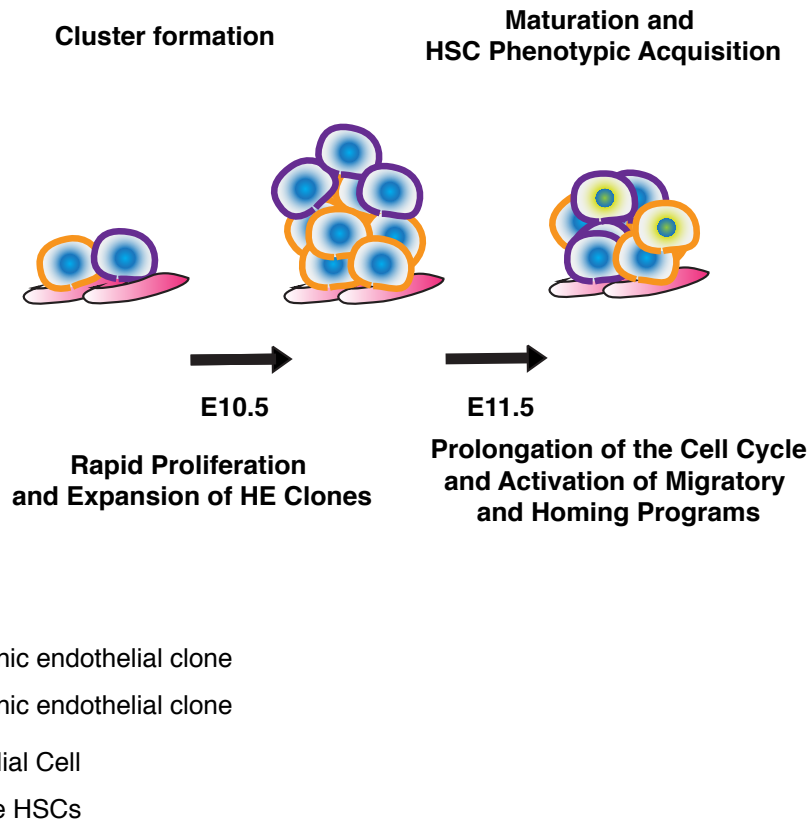


**Figure 13. Model of cluster formation and maturation of IAHCs to HSCs.**

(A) Schema depicting a model of IAHC formation and maturation. During the hemogenic window (E10-E11), distinct hemogenic clones are present in the dorsal aorta which undergo rapid proliferation forming polyclonal IAHCs. Following formation of an IAHC, cells undergo maturation towards an HSPC phenotype which may include prolongation of the cell cycle and activation of migratory and homing programs.

## References

1. Marcelo KL, Goldie LC, Hirschi KK. Regulation of endothelial cell differentiation and specification. *Circ Res*. 2013;112(9):1272-1287. doi:10.1161/CIRCRESAHA.113.300506.
2. Orkin SH, Zon LI. Hematopoiesis: an evolving paradigm for stem cell biology. *Cell*. 2008;132(4):631-644. doi:10.1016/j.cell.2008.01.025.
3. Palis J, Yoder MC. Yolk-sac hematopoiesis: the first blood cells of mouse and man. *Exp Hematol*. 2001;29(8):927-936.
4. Fantoni A, la Chapelle de A, Rifkind RA, Marks PA. Erythroid cell development in fetal mice: Synthetic capacity for different proteins. *Journal of Molecular Biology*. 1968;33(1):79-91. doi:10.1016/0022-2836(68)90282-9.
5. Brotherton TW, Chui DH, Gauldie J, Patterson M. Hemoglobin ontogeny during normal mouse fetal development. *Proc Natl Acad Sci USA*. 1979;76(6):2853-2857. doi:10.1073/pnas.76.6.2853.
6. Eichmann A, Corbel C, Nataf V, Vaigot P, Bréant C, Le Douarin NM. Ligand-dependent development of the endothelial and hemopoietic lineages from embryonic mesodermal cells expressing vascular endothelial growth factor receptor 2. *Proc Natl Acad Sci USA*. 1997;94(10):5141-5146.
7. Takahashi K, Naito M. Development, differentiation, and proliferation of macrophages in the rat yolk sac. *Tissue and Cell*. 1993;25(3):351-362. doi:10.1016/0040-8166(93)90077-X.
8. Xie X, Chan RJ, Johnson SA, et al. Thrombopoietin promotes mixed lineage and megakaryocytic colony-forming cell growth but inhibits primitive and definitive erythropoiesis in cells isolated from early murine yolk sacs. *Blood*. 2003;101(4):1329-1335. doi:10.1182/blood-2002-05-1468.
9. Krebs LT, Xue Y, Norton CR, et al. Characterization of Notch3-deficient mice: normal embryonic development and absence of genetic interactions with a Notch1 mutation. *Genesis*. 2003;37(3):139-143. doi:10.1002/gene.10241.
10. Johnson GR, Barker DC. Erythroid progenitor cells and stimulating factors during murine embryonic and fetal development. *Exp Hematol*. 1985;13(3):200-208.
11. Wong PM, Clarke BJ, Carr DH, Chui DH. Adult hemoglobins are synthesized in erythroid colonies in vitro derived from murine circulating hemopoietic progenitor cells during embryonic development. *Proc Natl Acad Sci USA*. 1982;79(9):2952-2956.
12. Schulz C, Gomez Perdiguero E, Chorro L, et al. A lineage of myeloid cells independent of Myb and hematopoietic stem cells. *Science*. 2012;336(6077):86-

90. doi:10.1126/science.1219179.
13. Ottersbach K, Dzierzak E. Analysis of the mouse placenta as a hematopoietic stem cell niche. *Methods Mol Biol.* 2009;538(Chapter 17):335-346. doi:10.1007/978-1-59745-418-6\_17.
  14. Gekas C, Dieterlen-Lièvre F, Orkin SH, Mikkola HKA. The placenta is a niche for hematopoietic stem cells. *Dev Cell.* 2005;8(3):365-375. doi:10.1016/j.devcel.2004.12.016.
  15. Alvarez-Silva M, Belo-Diabangouaya P, Salaün J, Dieterlen-Lièvre F. Mouse placenta is a major hematopoietic organ. *Development.* 2003;130(22):5437-5444. doi:10.1242/dev.00755.
  16. Müller AM, Medvinsky A, Strouboulis J, Grosveld F, Dzierzak E. Development of hematopoietic stem cell activity in the mouse embryo. *Immunity.* 1994;1(4):291-301.
  17. Medvinsky A, Dzierzak E. Definitive hematopoiesis is autonomously initiated by the AGM region. *Cell.* 1996;86(6):897-906.
  18. de Bruijn MF, Speck NA, Peeters MC, Dzierzak E. Definitive hematopoietic stem cells first develop within the major arterial regions of the mouse embryo. *EMBO J.* 2000;19(11):2465-2474. doi:10.1093/emboj/19.11.2465.
  19. Morrison SJ, Hemmati HD, Wandycz AM, Weissman IL. The purification and characterization of fetal liver hematopoietic stem cells. *Proc Natl Acad Sci USA.* 1995;92(22):10302-10306.
  20. Coşkun S, Chao H, Vasavada H, et al. Development of the fetal bone marrow niche and regulation of HSC quiescence and homing ability by emerging osteolineage cells. *Cell Rep.* 2014;9(2):581-590. doi:10.1016/j.celrep.2014.09.013.
  21. Jaffredo T, Gautier R, Eichmann A, Dieterlen-Lièvre F. Intraaortic hemopoietic cells are derived from endothelial cells during ontogeny. *Development.* 1998;125(22):4575-4583.
  22. Zovein AC, Hofmann JJ, Lynch M, et al. Fate tracing reveals the endothelial origin of hematopoietic stem cells. *Cell Stem Cell.* 2008;3(6):625-636. doi:10.1016/j.stem.2008.09.018.
  23. Sabin FR. *Preliminary Note on the Differentiation of Angioblasts and the Method by Which They Produce Blood-Vessels, Blood-Plasma and Red Blood-Cells as Seen in the Living Chick.* 1917. Vol 11. Mary Ann Liebert, Inc.; 2002:5-7. doi:10.1089/152581602753448496.
  24. Lancrin C, Sroczynska P, Stephenson C, Allen T, Kouskoff V, Lacaud G. The

- haemangioblast generates haematopoietic cells through a haemogenic endothelium stage. *Nature*. 2009;457(7231):892-895. doi:10.1038/nature07679.
25. Bertrand JY, Chi NC, Santoso B, Teng S, Stainier DYR, Traver D. Haematopoietic stem cells derive directly from aortic endothelium during development. *Nature*. 2010;464(7285):108-111. doi:10.1038/nature08738.
  26. Boisset J-C, van Cappellen W, Andrieu-Soler C, Galjart N, Dzierzak E, Robin C. In vivo imaging of haematopoietic cells emerging from the mouse aortic endothelium. *Nature*. 2010;464(7285):116-120. doi:10.1038/nature08764.
  27. North T, Gu TL, Stacy T, et al. Cbfa2 is required for the formation of intra-aortic hematopoietic clusters. *Development*. 1999;126(11):2563-2575.
  28. de Bruijn MFTR, Ma X, Robin C, Ottersbach K, Sanchez M-J, Dzierzak E. Hematopoietic stem cells localize to the endothelial cell layer in the midgestation mouse aorta. *Immunity*. 2002;16(5):673-683.
  29. Ottersbach K, Dzierzak E. The murine placenta contains hematopoietic stem cells within the vascular labyrinth region. *Dev Cell*. 2005;8(3):377-387. doi:10.1016/j.devcel.2005.02.001.
  30. de Bruijn MF, Peeters MC, Luteijn T, Visser P, Speck NA, Dzierzak E. CFU-S(11) activity does not localize solely with the aorta in the aorta-gonad-mesonephros region. *Blood*. 2000;96(8):2902-2904.
  31. Gordon-Keylock S, Sobiesiak M, Rybtsov S, Moore K, Medvinsky A. Mouse extraembryonic arterial vessels harbor precursors capable of maturing into definitive HSCs. *Blood*. 2013;122(14):2338-2345. doi:10.1182/blood-2012-12-470971.
  32. Nakano H, Liu X, Arshi A, et al. Haemogenic endocardium contributes to transient definitive haematopoiesis. *Nat Commun*. 2013;4:1564. doi:10.1038/ncomms2569.
  33. Yzaguirre AD, Padmanabhan A, de Groh ED, et al. Loss of neurofibromin Ras-GAP activity enhances the formation of cardiac blood islands in murine embryos. *Elife*. 2015;4:e07780. doi:10.7554/eLife.07780.
  34. Li Z, Lan Y, He W, et al. Mouse embryonic head as a site for hematopoietic stem cell development. *Cell Stem Cell*. 2012;11(5):663-675. doi:10.1016/j.stem.2012.07.004.
  35. Yzaguirre AD, Speck NA. Insights into blood cell formation from hemogenic endothelium in lesser-known anatomic sites. *Dev Dyn*. 2016;245(10):1011-1028. doi:10.1002/dvdy.24430.
  36. Kissa K, Herbomel P. Blood stem cells emerge from aortic endothelium by a novel type of cell transition. *Nature*. 2010;464(7285):112-115. doi:10.1038/nature08761.

37. Chen MJ, Yokomizo T, Zeigler BM, Dzierzak E, Speck NA. Runx1 is required for the endothelial to haematopoietic cell transition but not thereafter. *Nature*. 2009;457(7231):887-891. doi:10.1038/nature07619.
38. Solaimani Kartalaei P, Yamada-Inagawa T, Vink CS, et al. Whole-transcriptome analysis of endothelial to hematopoietic stem cell transition reveals a requirement for Gpr56 in HSC generation. *J Exp Med*. 2015;212(1):93-106. doi:10.1084/jem.20140767.
39. Taoudi S, Gonneau C, Moore K, et al. Extensive hematopoietic stem cell generation in the AGM region via maturation of VE-cadherin+CD45+ pre-definitive HSCs. *Cell Stem Cell*. 2008;3(1):99-108. doi:10.1016/j.stem.2008.06.004.
40. Yokomizo T, Dzierzak E. Three-dimensional cartography of hematopoietic clusters in the vasculature of whole mouse embryos. *Development*. 2010;137(21):3651-3661. doi:10.1242/dev.051094.
41. Taylor E, Taoudi S, Medvinsky A. Hematopoietic stem cell activity in the aorta-gonad-mesonephros region enhances after mid-day 11 of mouse development. *Int J Dev Biol*. 2010;54(6-7):1055-1060. doi:10.1387/ijdb.103152et.
42. Boisset J-C, Clapes T, Klaus A, et al. Progressive maturation toward hematopoietic stem cells in the mouse embryo aorta. *Blood*. 2015;125(3):465-469. doi:10.1182/blood-2014-07-588954.
43. Arora N, Wenzel PL, McKinney-Freeman SL, et al. Effect of developmental stage of HSC and recipient on transplant outcomes. *Dev Cell*. 2014;29(5):621-628. doi:10.1016/j.devcel.2014.04.013.
44. Cai Z, de Bruijn M, Ma X, et al. Haploinsufficiency of AML1 affects the temporal and spatial generation of hematopoietic stem cells in the mouse embryo. *Immunity*. 2000;13(4):423-431.
45. Wang Q, Stacy T, Binder M, Marín-Padilla M, Sharpe AH, Speck NA. Disruption of the Cbfa2 gene causes necrosis and hemorrhaging in the central nervous system and blocks definitive hematopoiesis. *Proc Natl Acad Sci USA*. 1996;93(8):3444-3449.
46. Muzumdar MD, Tasic B, Miyamichi K, Li L, Luo L. A global double-fluorescent Cre reporter mouse. *Genesis*. 2007;45(9):593-605. doi:10.1002/dvg.20335.
47. Livet J, Weissman TA, Kang H, et al. Transgenic strategies for combinatorial expression of fluorescent proteins in the nervous system. *Nature*. 2007;450(7166):56-62. doi:10.1038/nature06293.
48. Wang Y, Nakayama M, Pitulescu ME, et al. Ephrin-B2 controls VEGF-induced angiogenesis and lymphangiogenesis. *Nature*. 2010;465(7297):483-486. doi:10.1038/nature09002.

49. Madisen L, Zwingman TA, Sunkin SM, et al. A robust and high-throughput Cre reporting and characterization system for the whole mouse brain. *Nat Neurosci.* 2010;13(1):133-140. doi:10.1038/nn.2467.
50. Boisset J-C, Andrieu-Soler C, van Cappellen WA, Clapes T, Robin C. Ex vivo time-lapse confocal imaging of the mouse embryo aorta. *Nat Protoc.* 2011;6(11):1792-1805. doi:10.1038/nprot.2011.401.
51. Wilkinson AC, Kawata VKS, Schütte J, et al. Single-cell analyses of regulatory network perturbations using enhancer-targeting TALEs suggest novel roles for PU.1 during haematopoietic specification. *Development.* 2014;141(20):4018-4030. doi:10.1242/dev.115709.
52. Huang G, Zhang P, Hirai H, et al. PU.1 is a major downstream target of AML1 (RUNX1) in adult mouse hematopoiesis. *Nat Genet.* 2008;40(1):51-60. doi:10.1038/ng.2007.7.
53. Cappella P, Gasparri F, Pulici M, Moll J. A novel method based on click chemistry, which overcomes limitations of cell cycle analysis by classical determination of BrdU incorporation, allowing multiplex antibody staining. *Cytometry A.* 2008;73(7):626-636. doi:10.1002/cyto.a.20582.
54. Buck SB, Bradford J, Gee KR, Agnew BJ, Clarke ST, Salic A. Detection of S-phase cell cycle progression using 5-ethynyl-2'-deoxyuridine incorporation with click chemistry, an alternative to using 5-bromo-2'-deoxyuridine antibodies. *BioTechniques.* 2008;44(7):927-929. doi:10.2144/000112812.
55. Scholzen T, Gerdes J. The Ki-67 protein: from the known and the unknown. *J Cell Physiol.* 2000;182(3):311-322. doi:10.1002/(SICI)1097-4652(200003)182:3<311::AID-JCP1>3.0.CO;2-9.
56. Nomura T, Gotoh H, Ono K. Changes in the regulation of cortical neurogenesis contribute to encephalization during amniote brain evolution. *Nat Commun.* 2013;4:2206. doi:10.1038/ncomms3206.
57. Martynoga B, Morrison H, Price DJ, Mason JO. Foxg1 is required for specification of ventral telencephalon and region-specific regulation of dorsal telencephalic precursor proliferation and apoptosis. *Developmental Biology.* 2005;283(1):113-127. doi:10.1016/j.ydbio.2005.04.005.
58. Chen MJ, Li Y, De Obaldia ME, et al. Erythroid/myeloid progenitors and hematopoietic stem cells originate from distinct populations of endothelial cells. *Cell Stem Cell.* 2011;9(6):541-552. doi:10.1016/j.stem.2011.10.003.
59. Henninger J, Santoso B, Hans S, et al. Clonal fate mapping quantifies the number of haematopoietic stem cells that arise during development. *Nat Cell Biol.* 2016;19(1):17-27. doi:10.1038/ncb3444.

60. Eilken HM, Nishikawa S-I, Schroeder T. Continuous single-cell imaging of blood generation from haemogenic endothelium. *Nature*. 2009;457(7231):896-900. doi:10.1038/nature07760.
61. Patel SR, Hartwig JH, Italiano JE. The biogenesis of platelets from megakaryocyte proplatelets. *J Clin Invest*. 2005;115(12):3348-3354. doi:10.1172/JCI26891.
62. Xu MJ, Matsuoka S, Yang FC, et al. Evidence for the presence of murine primitive megakaryocytopoiesis in the early yolk sac. *Blood*. 2001;97(7):2016-2022. doi:10.1182/blood.V97.7.2016.
63. Zhao M, Perry JM, Marshall H, et al. Megakaryocytes maintain homeostatic quiescence and promote post-injury regeneration of hematopoietic stem cells. *Nat Med*. 2014;20(11):1321-1326. doi:10.1038/nm.3706.
64. Bruns I, Lucas D, Pinho S, et al. Megakaryocytes regulate hematopoietic stem cell quiescence through CXCL4 secretion. *Nat Med*. 2014;20(11):1315-1320. doi:10.1038/nm.3707.
65. Nygren JM, Bryder D, Jacobsen SEW. Prolonged cell cycle transit is a defining and developmentally conserved hemopoietic stem cell property. *J Immunol*. 2006;177(1):201-208.
66. Pietras EM, Warr MR, Passegué E. Cell cycle regulation in hematopoietic stem cells. *J Cell Biol*. 2011;195(5):709-720. doi:10.1083/jcb.201102131.
67. Bowie MB, Kent DG, Dykstra B, et al. Identification of a new intrinsically timed developmental checkpoint that reprograms key hematopoietic stem cell properties. *Proc Natl Acad Sci USA*. 2007;104(14):5878-5882. doi:10.1073/pnas.0700460104.
68. Ding L, Morrison SJ. Haematopoietic stem cells and early lymphoid progenitors occupy distinct bone marrow niches. *Nature*. 2013;495(7440):231-235. doi:10.1038/nature11885.
69. Kunisaki Y, Bruns I, Scheiermann C, et al. Arteriolar niches maintain haematopoietic stem cell quiescence. *Nature*. 2013;502(7473):637-643. doi:10.1038/nature12612.
70. Arai F, Hirao A, Ohmura M, et al. Tie2/angiopoietin-1 signaling regulates hematopoietic stem cell quiescence in the bone marrow niche. *Cell*. 2004;118(2):149-161. doi:10.1016/j.cell.2004.07.004.
71. Sugimura R, He XC, Venkatraman A, et al. Noncanonical Wnt signaling maintains hematopoietic stem cells in the niche. *Cell*. 2012;150(2):351-365. doi:10.1016/j.cell.2012.05.041.

72. Wilson A, Murphy MJ, Oskarsson T, et al. c-Myc controls the balance between hematopoietic stem cell self-renewal and differentiation. *Genes Dev.* 2004;18(22):2747-2763. doi:10.1101/gad.313104.
73. Gothot A, Pyatt R, McMahel J, Rice S, Srour EF. Functional heterogeneity of human CD34(+) cells isolated in subcompartments of the G0 /G1 phase of the cell cycle. *Blood.* 1997;90(11):4384-4393.
74. Fleming WH, Alpern EJ, Uchida N, Ikuta K, Spangrude GJ, Weissman IL. Functional heterogeneity is associated with the cell cycle status of murine hematopoietic stem cells. *J Cell Biol.* 1993;122(4):897-902.
75. Habibian HK, Peters SO, Hsieh CC, et al. The fluctuating phenotype of the lymphohematopoietic stem cell with cell cycle transit. *J Exp Med.* 1998;188(2):393-398.
76. Glimm H, Oh IH, Eaves CJ. Human hematopoietic stem cells stimulated to proliferate in vitro lose engraftment potential during their S/G(2)/M transit and do not reenter G(0). *Blood.* 2000;96(13):4185-4193.
77. Orschell-Traycoff CM, Hiatt K, Dagher RN, Rice S, Yoder MC, Srour EF. Homing and engraftment potential of Sca-1(+)lin(-) cells fractionated on the basis of adhesion molecule expression and position in cell cycle. *Blood.* 2000;96(4):1380-1387.
78. Sakaue-Sawano A, Kurokawa H, Morimura T, et al. Visualizing spatiotemporal dynamics of multicellular cell-cycle progression. *Cell.* 2008;132(3):487-498. doi:10.1016/j.cell.2007.12.033.
79. Cheshier SH, Morrison SJ, Liao X, Weissman IL. In vivo proliferation and cell cycle kinetics of long-term self-renewing hematopoietic stem cells. *Proc Natl Acad Sci USA.* 1999;96(6):3120-3125.
80. Dykstra B, Kent D, Bowie M, et al. Long-term propagation of distinct hematopoietic differentiation programs in vivo. *Cell Stem Cell.* 2007;1(2):218-229. doi:10.1016/j.stem.2007.05.015.
81. Challen GA, Boles NC, Chambers SM, Goodell MA. Distinct hematopoietic stem cell subtypes are differentially regulated by TGF-beta1. *Cell Stem Cell.* 2010;6(3):265-278. doi:10.1016/j.stem.2010.02.002.
82. Kowalczyk MS, Tirosh I, Heckl D, et al. Single-cell RNA-seq reveals changes in cell cycle and differentiation programs upon aging of hematopoietic stem cells. *Genome Res.* 2015;25(12):1860-1872. doi:10.1101/gr.192237.115.
83. McKinney-Freeman S, Cahan P, Li H, et al. The transcriptional landscape of hematopoietic stem cell ontogeny. *Cell Stem Cell.* 2012;11(5):701-714. doi:10.1016/j.stem.2012.07.018.

84. Li Y, Esain V, Teng L, et al. Inflammatory signaling regulates embryonic hematopoietic stem and progenitor cell production. *Genes Dev.* 2014;28(23):2597-2612. doi:10.1101/gad.253302.114.
85. Espín-Palazón R, Stachura DL, Campbell CA, et al. Proinflammatory signaling regulates hematopoietic stem cell emergence. *Cell.* 2014;159(5):1070-1085. doi:10.1016/j.cell.2014.10.031.
86. Sawamiphak S, Kontarakis Z, Stainier DYR. Interferon gamma signaling positively regulates hematopoietic stem cell emergence. *Dev Cell.* 2014;31(5):640-653. doi:10.1016/j.devcel.2014.11.007.
87. He Q, Zhang C, Wang L, et al. Inflammatory signaling regulates hematopoietic stem and progenitor cell emergence in vertebrates. *Blood.* 2015;125(7):1098-1106. doi:10.1182/blood-2014-09-601542.
88. Ratajczak J, Reza R, Kucia M, et al. Mobilization studies in mice deficient in either C3 or C3a receptor (C3aR) reveal a novel role for complement in retention of hematopoietic stem/progenitor cells in bone marrow. *Blood.* 2004;103(6):2071-2078. doi:10.1182/blood-2003-06-2099.
89. Reza R, Mastellos D, Majka M, et al. Functional receptor for C3a anaphylatoxin is expressed by normal hematopoietic stem/progenitor cells, and C3a enhances their homing-related responses to SDF-1. *Blood.* 2003;101(10):3784-3793. doi:10.1182/blood-2002-10-3233.
90. Lee HM, Wu W, Wysoczynski M, et al. Impaired mobilization of hematopoietic stem/progenitor cells in C5-deficient mice supports the pivotal involvement of innate immunity in this process and reveals novel promobilization effects of granulocytes. *Leukemia.* 2009;23(11):2052-2062. doi:10.1038/leu.2009.158.
91. Jalili A, Marquez-Curtis L, Shirvaikar N, Wysoczynski M, Ratajczak M, Janowska-Wieczorek A. Complement C1q enhances homing-related responses of hematopoietic stem/progenitor cells. *Transfusion.* 2010;50(9):2002-2010. doi:10.1111/j.1537-2995.2010.02664.x.

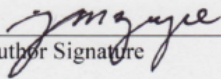
Prepare in duplicate

**Publishing Agreement**

*It is the policy of the University to encourage the distribution of all theses, dissertations, and manuscripts. Copies of all UCSF theses, dissertations, and manuscripts will be routed to the library via the Graduate Division. The library will make all theses, dissertations, and manuscripts accessible to the public and will preserve these to the best of their abilities, in perpetuity.*

**Please sign the following statement:**

*I hereby grant permission to the Graduate Division of the University of California, San Francisco to release copies of my thesis, dissertation, or manuscript to the Campus Library to provide access and preservation, in whole or in part, in perpetuity.*

  
\_\_\_\_\_  
Author Signature

3/20/17  
\_\_\_\_\_  
Date